POLITECNICO DI TORINO

Master Degree course in Aerospace Engineering

Master Degree Thesis

Experimental study of a vertical axis wind turbine on multi-storey building models

Supervisors
Prof. Tania Bracchi
Prof. Gaetano Iuso

Candidate
Michele Modina

Academic Year 2022-2023

Preface

This thesis work was carried out at the Department of Energy and Process Engineering at Norwegian University of Science and Technology in Trondheim. The experiments were conducted in October 2022 in collaboration with Kris Michael Avellana Gabriel, a master student at NTNU.

Trondheim, April 2023
Michele Modina

Acknowledgements

Un sincero ringraziamento è rivolto alla professoressa Tania Bracchi per l'attenzione e la passione con cui si è dedicata al mio lavoro di tesi. L'opportunità di collaborare con lei e l'Experimental Fluids Group dell'NTNU mi ha permesso di capire cosa significa fare ricerca tramite la sperimentazione fluidodinamica. Un grande grazie è dedicato anche al professor Gaetano Iuso che dall'Italia mi ha seguito e supportato in questi mesi. Next, I'd like to thank my friend Kris. Through our teamwork it was easier to study the experimental campaign of the thesis. Furthermore, working together on the project was fun. I would also like to express my gratitude to all my friends here in Trondheim from Vannkraftlaboratoriet and the St.Augustin group.

Per il sostegno che ho sempre ricevuto durante tutti questi anni di studio non posso che ringraziare anche tutta la mia famiglia. In particolare, mio babbo per il suo supporto costante e mia mamma che con il suo carattere tenace mi ha stimolato a implicarmi sempre al 110% in ciò che son chiamato a fare.

Sono grato anche dell'incontro e dell'amicizia con il CLU e con i compagni corso; in modo speciale Co, Zanna e Gaia. Con tutti voi, durante questi anni di università, mi sono sempre sentito accompagnato e posso dire di essere cresciuto integralmente come persona.

Infine, un grande grazie ad Eli, per tutto quello che abbiamo condiviso e la serietà con cui ci siamo aiutati a camminare insieme, difronte allo studio e ai nostri desideri per il futuro.

Abstract

Nowadays, it is becoming more and more crucial to generate electricity without emitting harmful emissions. Installing small vertical axis wind turbines on the roof of the buildings can be a solution for energy demand in urban areas. The challenge is that there are many different aspects that can impact the operation of a roof-mounted wind turbine. In order to assess the potential of urban wind it is essential to comprehend how these variables affect the turbine's performance. The purpose of this study is to examine how the performances are affected both by the wind turbine position on the roof, the building height and the turbine height. In order to do this the performances of a Savonius wind turbine model, mounted on the top of tandem configuration of two multi-storey building models, has been measured at six streamwise positions. Additionally, the flow field over the roof, without the turbines, was measured at several points with a Cobra Probe in order to comprehend the flow field in which the turbine is situated. In general it could be noticed that the roof-mounted wind turbine on a high-rise building are worst, compared to a lower building, when placed on the windward structure, whereas they are comparable when located on the leeward building.

Contents

Chapter 1

Introduction

1.1 Motivation

The International Energy Agency (IEA) claims that the world is currently experiencing an energy crisis of unparalleled magnitude and complexity, IEA [2022]. There are numerous causes at play in this situation. In the past two years a lot has happened, including the pandemic and the Russian invasion of Ukraine. Due to the pandemic and the suspension of numerous work activities in 2020 energy demand decreased. However, in 2021 there has been a significant economic recovery with a rise in nearly every state's GDP. Due to this reality, the demand for energy has expanded globally in an unprecedented way, resulting in the highest recorded CO2 emissions of about 36 Gt, IEA [2022]. The graph of figure 1.1 shows the percentage variation of CO2 emissions from the fossil fuel combastion over the past three years. However, at the same time the clean power production increased by 500

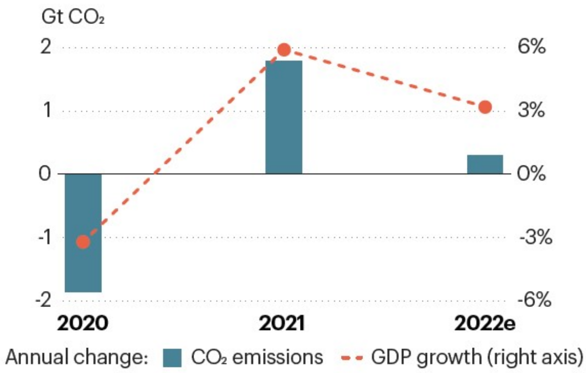

Figure 1.1: Percentage variation of CO2 emissions from global fossil fuel combustion in the last three years, figure from IEA [2022]

TWh in 2021 (compared to year 2020) reaching the total clean power production of 8000 TWh, the highest amount ever recorded in the world. Indeed, in accordance with the 2015 Paris Agreements and with the "Net Zero CO2 emission goal by 2050" investments in renewable energy were boosted in 2021, IEA [2021], especially in Europe. Since Russia invaded Ukraine in February 2022, the situation has grown even more complicated, see figure 1.2. Energy costs have indeed risen across all the world, and it is now clearer than ever that greater investment will be required to enable many nations to achieve energy independence, particularly in the production of renewable energy. Wind power undoubtedly makes an important contribution to the shift towards sustainable energy sources.

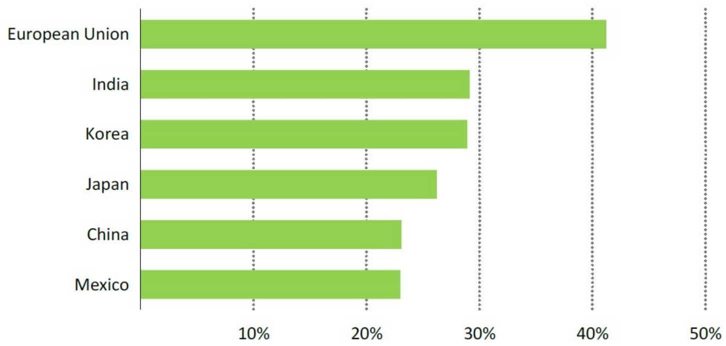

Figure 1.2: Increases in power generation costs in the first half of 2022, figure from IEA [2022]

Indeed, the total installed wind capacity worldwide in 2020 including both onshore and offshore wind turbines was 743 GW, Gil-Garcìa et al. [2022]. Over the time, the average size of wind turbines has increased, and as a result they are frequently located far from urban area where a significant amount of energy is consumed. Therefore, significant expenses are required to build power transmission facilities, Jooss [2022]. In urban areas new options for decentralized electricity production free from reliance on the grid and free from transmission losses are provided by small-scale vertical axis wind turbine VAWT, Gil-Garcìa et al. [2022]. Urban areas have very turbulent and multidirectional winds but VAWT are a potential technology for urban applications, IRENA [2020]. The Savonius and Darrieus turbines are the most popular vertical-axis wind turbines. The typical size of these turbines for urban applications ranges from 1 to 6 meters in height and a few meters in diameter, Jooss et al. [2022a]. There are several benefits to using VAWT to generate energy without emissions, but it can be difficult to understand their peak performance. In fact, the flow field in an urban area is quite complex, and factors such as turbulence intensity, wind speed, and flow direction have a significant impact on the amount of power generated by the turbine. This work examines how the performance of a turbine installed on a building's roof might be impacted by the buildings' height. To achieve this goal, an experimental investigation is carried out in NTNU's wind tunnel. On the test section of the wind tunnel, two scaled-down buildings (square cylinders) are specifically arranged in tandem. For twelve study cases, a mini VAWT (3 cm height and 4 cm of diameter) is installed on the roof of the buildings in six distinct positions and two different heights. First the flow field without the turbine is analysed. Then the Cp-Tsr curves are acquired using an electrical setup. The effects of several variables such as wind speed and direction, turbine height, and turbulence, on a Savonius turbine mounted on a roof are already examined in Jooss [2022]. This thesis wants to improve on the results that were obtained by Jooss [2022].

1.2 Background

First of all, it is essential to comprehend the flow field around the two model structures. The literature on flow fields of various building and palace configurations is extensive. In Dar et al. [2022] an idealized urban canopy model is set up inside the test section of a wind tunnel to simulate an urban boundary layer. The idea was to have a taller building surrounded by a set of smaller ones. The authors analysed how minor modifications to roof edge shape influence the power performance of the turbine placed on the roof. The results show that the best power output is reached with a sharp edge of the cube. Instead, a 2D numerical simulation of a building with the same height to width ratio as current experiments is studied in Toja-Silva et al. [2013]. A large vortex that may be helpful or harmful to the operation of the roof-mounted turbine is specifically depicted on the top of the structures. The works of Martinuzzi and Havel [1999] and Martinuzzi and Havel [2004] permit to understand the flow around a tandem configuration of buildings. In the first study they analysed what is the effect of the spacing between the first and the second buildings. In the second study they worked more in detail on cubes in tandem configuration with a specific space of two times the edge of the cubes because they found that this distance is interesting. Indeed, the drag coefficient (based on the frontal area and free stream velocity) shows an abrupt drop. In Jooss et al. [2022a] and Jooss et al. [2022b] it is also set like space between the two cube a distance of 2H (where H is the edge dimension of the cube). Therefore, the first step is understand the flow field around structures similar to the current experiment and later understand how the wind turbine works over these buildings. It's possible to observe relevants results also in McClean and Sumner [2014] where the authors studied through an experimental analysis the effect of the aspect ratio A.R. (height over width) on a square prism. The authors tested an aspect ratios between 3 and 11. It was found that each Cd (drag coefficient) was lower compared to the infinite square prism (especially between A.R. of 3 and 5 the Cd is much lower). Hence in that article is put in evidence how the height of the buildings influences the flow field around it. In Sum [2004] the researchers studied the influence of the aspect ratio on the flow field around a building partially placed in a turbulent boundary layer. Here the authors show the relation between the wake behind the model-building and its aspect ratio. The influence of the wake on the leeward building is clearly important in case of the configuration of two buildings in tandem, like in the current experiments. In Jooss [2022] the author studies the influence of free-stream turbulence on the performance of small turbine installed over model buildings and it was found that the amount of turbulence in the intake significantly affects both the flow field and the turbine's power output. Indeed, the area of recirculating flow over the cube becomes narrower as the turbulence intensity of free stream flow increases. In Ledo et al. [2011] the scientists show that the roof shape with the best velocities profile is flat. For this reason in the current experiment the roof of the model buildings have the same shape. Indeed, a flat roof has a lower turbulence intensity compared to the other roof (pyramidal and pitched roof). In Jooss et al. [2022a] the researchers show that for predicting the extract's power of a vertical axis wind turbine it is essential to study the flow field with the presence of a turbine. Indeed, the turbine affects the flow field and consequently its power output. In that study, a model of VAWT was placed in the wind tunnel over an idealized scaled down model buildings subsequently the flow fields with and without the turbine were recorded. The rotor has a negative impact on the flow field practically everywhere; the average velocity across the wind turbine's span is decreased, and the turbulence intensity is increased. In Jooss et al. [2022a] they tested the turbine on the top of each cube (at six different places: front, centre and back) and it is found that the power extracted from the wind turbine is higher on the frontal and central positions of the windward building, but it decreases on the back position. Another important result of this work is that on the leeward building the power increases from the front to the back position. The authors of Jooss et al. [2022b] examine many factors which affect the performance of the wind turbine, including the impact of the rotor's height, the location on the cube, and the impact of wind direction. The aim of that research was to study two distinct heights of turbine, six different locations on the cubes, and five different wind directions. From that work the high turbines give the best results in almost every positions and the most robust position adaptable to the major number of wind directions is the central one. Indeed, in this position for all the wind directions the high turbine has the higher Cp_{max} than Cp_{0max}. Another important analysis comes out from the research of Pagnini et al. [2015] where the authors studied two small wind turbines (HAWT and VAWT) installed in Savona Harbour. In this case they discovered that performances of the turbines are negative affected by turbulence intensities greater than 15%.

1.3 Objective and scope

At this point much work has been done by different researcher in different projects. However the micro wind power generation has still lot of open questions. Focusing on the works of Jooss et al. [2022b] and Jooss et al. [2022a] it's understandable the influence of many parameters (wind direction, turbine height and turbine positions) on the performance of a VAWT installed over a building. Nonetheless other parameters remain to analyze. The aim of this thesis is to analyze one of the unstudied parameters: the ratio between building height and turbine height. To attain this objective, tests have been conducted using higher building-models than what it has been used in Jooss et al. [2022b]. In that work the ratio between the turbine height h_t and the edge of the cube h was $h_t/h = 0.3$. The new value of the ratio is 0.15 (the half of the previous value) so it's possible to model a multistore building. Indeed, in Jooss et al. [2022a] the authors say that the average range of h_t/h (for three-storey buildings) is 0.08-0.62. This thesis contains a comparison between the results of the current experiments and the research of Jooss et al. [2022b]. Indeed the setups of the experiments are the same.

1.4 Outline

The current chapter provides informations about the motivation behind this project, the state of the art, and the scope of this thesis, which is to understand the flow field around a tandem configuration of two square cylinders and the performance of a small vertical wind turbine installed on them. In the first section of the next chapter there is a description of the urban boundary layer, which is crucial in comprehending the environment where the turbine is located and the flow around model-buildings of the same type used in the experiment. The second section of the chapter discuss the performance and operation parameters of wind turbines, particularly the Savonius wind turbine. The third chapter details the experimental setup and methods, including the location, instruments used to acquire the flow field and power from the turbine. The second-last chapter contains the results (including performance and flow field characteristics) and a comparison with previous studies. The thesis concludes with a summary of the findings and suggestions for future work.

Chapter 2

Theory

2.1 Urban flow field

2.1.1 Urban boundary layer

Low yearly mean wind speeds and high turbulent flow characterize the urban wind regime, KC et al. [2019]. Roughness characteristics in urban environments have a significant impact on key wind variables such as intensity turbulence, wind speed, and wind profile. Therefore, it is crucial to evaluate these aerodynamic features of urban locations critically and precisely when describing urban wind behaviour, Ishugah et al. [2014]. The parameters stated above will be examined in section 4.1 for the flow field analysed in this experiment. Urban morphology varies a lot across different cities, and this has a variety of effects on how wind flows over it. However, it's possible to divide the flow in the atmospheric boundary layer over urban areas into different regimes in which the wind has different characteristics. The names of these sublayers are: urban canopy, roughness sublayer, surface layer and outer layer. *Urban canopy* is the layer immediately over the ground and it extends between the terrain and the rooftop level. Here the flow is complex indeed the geometry of the canopy affects it. Over the urban canopy there is the *roughness sublayer* which has a thickness of $2 - 5H_b$ where H_b = height of building . In this layer the turbulence starts to homogenize the flow but it is still affected by the roughness elements. Over the roughness sublayer it is possible to find a flow where the turbulent mixing cancels the effects of individual urban structures and buildings. In this zone, called *surface layer*, the turbulent fluxes are constant with the height and the wind profile is logarithmic. In the end the outer part of the urban boundary layer is the *mixed layer*. In that layer the wind profile is no more logarithmic and the fluxes vary significantly with height Wang et al. [2014], Fernando [2010]. In figure 2.1 there is a pattern of the flow in the urban boundary layer.

The urban boundary layer is complex thus it is necessary to study it by different methodologies: laboratory, analytical, and high-resolution numerical analyses, Fernando [2010]. High computational costs and accurate models of the domain geometry are the main challenges of numerical simulation of urban wind enviroment, KC et al. [2019] . It is essential also to invest more in the direct measurement of wind data in urban areas because these measurements are typically challenging due to complex terrain and the

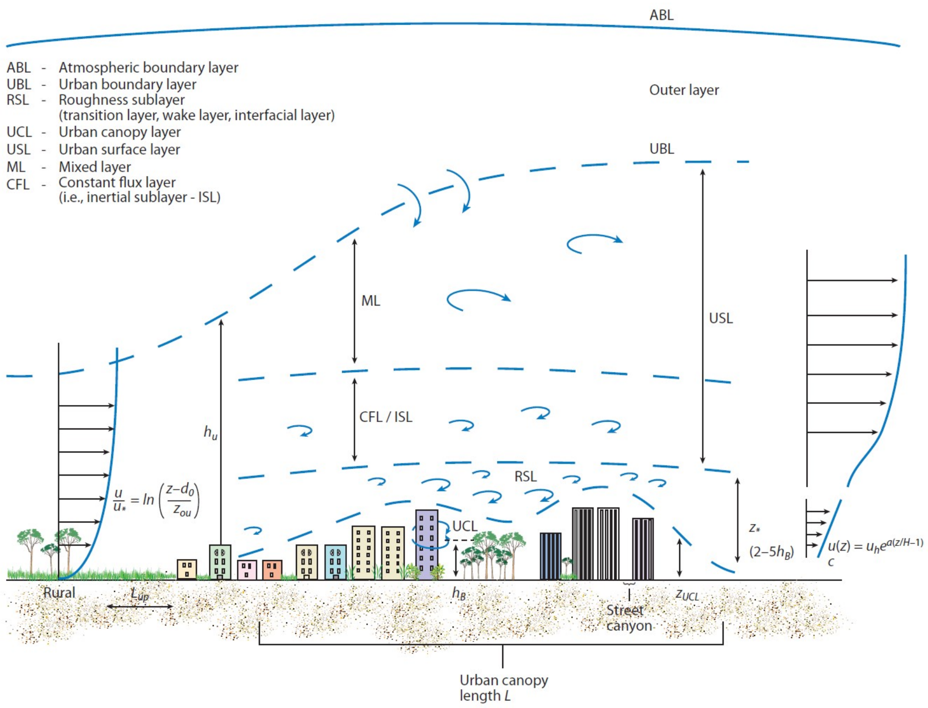

Figure 2.1: Urban boundary layer, figure from Fernando [2010]

unpredictable nature of wind, KC et al. [2019]. In literature it is possible to find some analytical model of flow in the urban boundary layer elaborated for the mesoscale models (weather forecast). For example, in Zajic [2006] the author cites a model for in-canopy velocity scale. The conclusion of this section is that the urban enviroment is complex and it is diffucult to fully understand its characteristics. Indeed, there are lot of factors which influence this type of flow. The high level of turbulence intensity affects the operability and the lifetime of wind turbines, Ledo et al. [2011]. On the other hand, it is essential to delve deeper into this as it is vital for improving the design and the efficiency of small wind turbines installed in urban areas.

2.1.2 Flow around buildings

Different kinds of studies on the flow around buildings exist in literature. Usually many of these studies, especially on tall palaces, are related to the estimation of wind loads exerted on the building's structure. There are also other studies where the authors try to replicate real configurations of urban environment like in Ledo et al. [2011], in Dar et al. [2022] or Sarkic Glumac et al. [2018]. These analyses focus on the flow over the building and what are the best configurations for installing wind turbines. The authors, in Sarkic Glumac et al. [2018] make an analysis of the flow over the roof of a building sorrounded by a configuration of other four high-rise buildings. They found that the upstream model highly affects the flow over the central building when the wind direction is 0°. The study of Dar et al. [2022] makes a comparative analysis of different edge of roof shape of a model building. The authors study a sharp edge, a rounded edge, and a solid fence. The sharp edge is the best shape. Indeed like it's stated in section 1.2, it permits to maximize the performance of a roof-top turbine. Abohela et al. [2013] analyse the influence of building roof shape (flat, wedged, pyramidal, barrel vaulted and spherical) on rooftop installed turbines. They conclude that the barrel vaulted roof it's the most appropriate for wind turbine. Contrary to Abohela et al. [2013], Ledo et al. [2011] state that turbines mounted on flat roof can be more efficient than on other roofs.

Mertens [2006] shows the flow field on the roof of a building, simulated through a 2D CFD analysis. How it is possible to see in figure 2.2, the flow separetes at the upwind edge of the building. A recirculation zone with high level of turbulence appears early after the separation of the flow. This region of the flow is interesting for this study because the micro wind turbine is partially submerged in it.

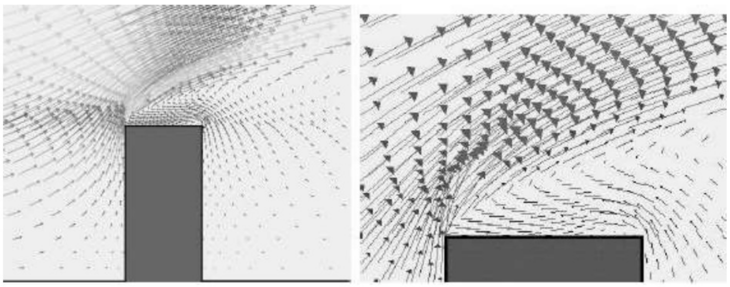

Figure 2.2: CFD 2D flow field over building, figure from Mertens [2006]

From figure 2.2 it is clear that the velocity vectors, over the recirculation zone, can't be considered parallel to the u component of the velocity. Indeed the velocity has a skew angle. Mertens [2006] states that the value of the skew angle depends on different factors: position, roughness of upwind area, dimensions of building, shape of upwind edge and yaw of the free stream wind.

The equilibrium of the force generated by the pressure gradient and the centrifugal force describe the recirculation zone over the building roof.

Wilson [1979] proposes a 3D model for estimating the size of the recirculation zone downwind of the leading edge of the building. L is a characteristic size of the upwind wall and the model utilizes it. Formula 2.1 express the value of L:

$$L = L_{small}^{\frac{2}{3}} L_{large}^{\frac{1}{3}} \tag{2.1}$$

In 2.1, L_{small} and L_{large} are respectively the smallest and the biggest crosswind dimensions of the building facade. The model of the recirculation zone is:

$$z = 0.28 D^{\frac{2}{3}} x^{\frac{1}{3}} \tag{2.2}$$

The empirical model is valid in the range of $0.1 < x/D < 0.4$.
Another interesting characteristic of the flow over the recirculation zone is put in evidence in Jooss et al. [2022a]. Indeed in this study the authors found that the flow field over the recirculation zone on the windward building experiences an increment on the velocity,

like it is possible to see in figure 2.3 (where U_c indicates the velocity component of the flow in the x-direction and U_∞ is the free-stream velocity). It means that the turbine can reach high performance if it's placed on the windward building on the zone where the flow speed increase (black vectors in the figure 2.3).

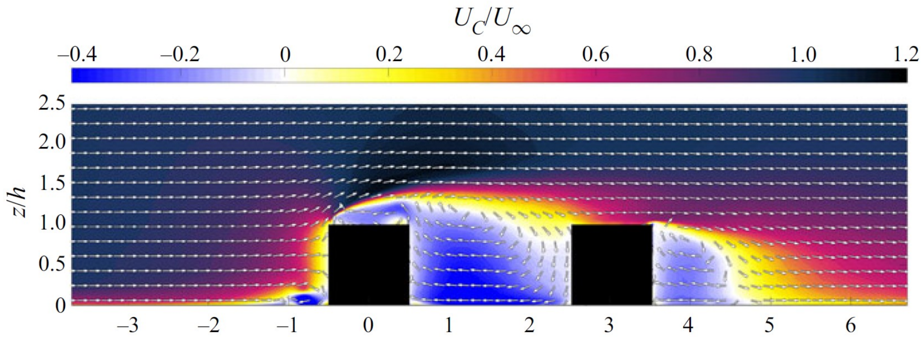

Figure 2.3: Flow field around the cubes at $Re = 80000$, figure from Jooss et al. [2022a]

At the end it is important to analyse the effect of the distance between the buildings. Relevant results can be found in Martinuzzi and Havel [1999] where the authors analyse the flow field around two cubes in the wind tunnel, varying the distance between them along the x-axis.

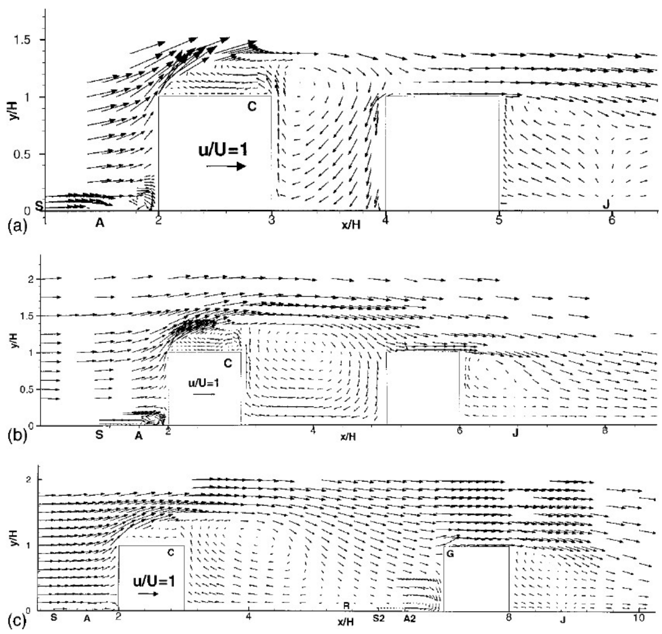

Figure 2.4: Flow field around the cubes at $Re = 22000$: a)$S/H = 1$, b)$S/H = 1$ and c)$S/H = 4$, figure from Martinuzzi and Havel [1999]

As already mentioned in section 1.2 the best configuration of the buildings is with the cubes at a distance which is two times the height. Indeed, how it can be seen in the figure 2.4b, for $S/H = 2$ (where S is the space between the cubes and H the height of the cube) the flow field is great. Indeed the flow detached from the windward building doesn't affect the flow over the leeward building. Furthermore the vortex created inside the concavity between the buildings is weak compared to $S/H = 1$.

2.1.3 Turbulence intensity

The performance (in term of power coefficient) of the Savounius turbine can be significantly reduced by the turbulence of the flow, Akwa et al. [2012]. In section 2.1.1 the turbulence is an important factor in the urban boundary layer and for this reason it's necessary to consider it. Thanks to the Reynolds Decomposition is possible to decompose the velocity vector in two parts: the mean velocity $|\overline{U}|$ and the fluctuation $u^{'}$. The decomposition of istantaneous velocity in the x-direction U is:

$$U = |\overline{U}| + u^{'} \tag{2.3}$$

In equation 2.3, the mean velocity is defined by the integral average:

$$\overline{U} = \frac{1}{T}\int_0^T U dt \tag{2.4}$$

In the end, through the two definitions, 2.3 and 2.4, it is possible to define the parameter by wich it's measured the turbulence around the building models in the current experiments. The last one is called turbulence intensity Iuu. The formula 2.5 defines the turbulence intensity along the x-direction:

$$I_{uu} = \frac{\sqrt{\overline{u'^2}}}{|\overline{U}|} \tag{2.5}$$

The numerator $\sqrt{\overline{u'^2}}$ of equation 2.5 represents the standard deviation of the velocity and the denominator $|\overline{U}|$ is the mean velocity. The measurements of the turbulence intensity in the current experiments are performed through the Cobra Proba and the TFI software.

2.2 Wind turbine

A wind turbine is a device that turns wind energy into electricity. The actual conversion process in modern wind turbines exploits the fundamental aerodynamic force of lift to produce a net positive torque on a rotating shaft, first producing mechanical power and then converting it to electricity. The horizontal axis wind turbine is currently the most used type of wind turbine (HAWT), in this case the axis of rotation is parallel to the terrain, Manwell [2009]. These kinds of turbines are usually used out of the city center, and they permit to reach high power output. On the other hands these types of turbines have some limits. For example, they produce lots of noise due to the dimensions of the blades and the high velocities reached at their tips. Moreover it's necessary a system for orientating the turbine with wind direction because it can generate more power if it is aligned to the flow direction. So, different types of rotors (more suitable for produce energy in urban area) were studied to avoid some of the last problems. These turbines are called VAWT (Vertical Axis Wind Turbine). They have lots of beneficial characteristics. They don't need a yaw mechanism, the efficiency in a turbulent flow is higher for them and they are easier than the other to install in small places, Jha and Jha [2010]. In this project it has been studied a VAWT, in particular a Savonius type.

2.2.1 Operating parameters

The most important and interesting parameter is the coefficient of power, also called Cp. It represents how much of the wind power is extracted by the rotor. The definition is:

$$C_P = \frac{P}{\frac{1}{2}\rho U^3 A} = \frac{RotorPower}{AvailablePower} \tag{2.6}$$

Where ρ is the density of the air, U is the velocity of the flow and A is the frontal area of the turbine. The denominator of the fraction represents the available power P_A in the wind and it comes from the definition of kinetic energy per unit of time:

$$P_A = \frac{1}{2}\frac{dm}{dt}U^2 = \frac{1}{2}\rho A U^3 \tag{2.7}$$

Indeed, $\frac{dm}{dt} = \rho A U$ by the continuity equation of fluid mechanics. The C_P coefficient is dimensionless and it represents the efficiency parameter when used to compare wind turbines of the same types with the same flow conditions. In case of horizontal axis wind turbine it is possible to define $C_{P,max} = 0.5926$. It is called Betz Limit, in honour of his inventor. This value derives by the application of the One dimensional Momentum Theory to an ideal turbine rotor. The theory assumes that:

- the flow is homogeneous, incompressible and steady;
- the number of blades is infinite;
- there aren't frictional drag and rotating wake;
- the thrust over the rotor area is uniform;
- the pressure far upstream and downstream of the disc area is the same of the undisturbed static ambient pressure.

Unfortunately, for the Savonius turbine the Betz limit is far from the real Cp that it can achive. Indeed the highest Cp value for a Savonius is between 0.2 and 0.3, instead for a HAWT could be over 0.45. The drag-driven turbines are less efficient than the lift-driven turbines because the drag force is function of the relative wind speed between the free stream velocity and the speed of the surface of the rotor. For the lift machine instead it's easy to reach realative wind velocity grater than the velocity of free stream velocity. Hence, the $C_{P,max}$ of the lift-driven turbine is usually higher than the ones of the drag-driven rotor. In figure 2.5 it's possible to see the C_P performances for different kind of turbines. The tip speed ratio is an important dimensionless parameter used for the wind turbine description. By definition, this parameter is:

$$\lambda = \frac{\Omega r}{U_\infty} = \frac{U_{tip}}{U_\infty} \tag{2.8}$$

In this case Ω represents the angular velocity, r the radius of the turbine and U_∞ the free stream velocity. The tip speed ratio is an expression of the noise level of the turbine and it is also useful to understand at what velocity the turbine is working. For more

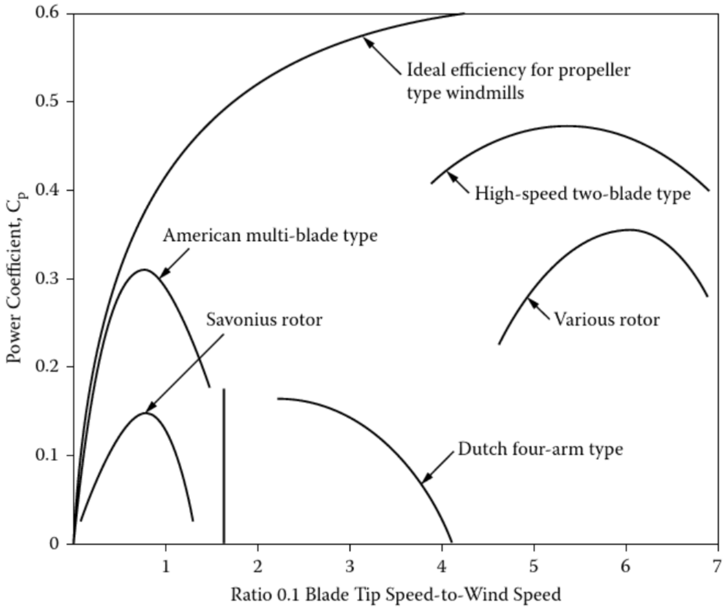

Figure 2.5: Cp-TSR curves of different wind turbines, figure from Jha and Jha [2010]

details regarding formulas 2.6, 2.7 and 2.8, it is possible to see Manwell [2009] and Wood [2011]. In the current experiments the rotor power P in the formula 2.6 and the angular velocity Ω in equation 2.8 result from the calculations with data acquired with different instruments, like is stated in section 3.3. First of all, in order to obtain the mechanical power is necessary to calculate the converted power with the formula:

$$P_c = Q_{em}\Omega \tag{2.9}$$

In formula 2.9 the angular velocity is $\Omega = \frac{RPM2\pi}{60}$. With the previous calculation it is possible to estimate the TSR, λ. In order to obtain Q_{em}, that represents the electromagnetic torque, it's necessary to measure the intensity of the current and multiply it by the coefficient K_t (the constant of the generator):

$$Q_{em} = K_t I \tag{2.10}$$

At the end the mechanical power P_m is:

$$P_m = P_c + P_f \tag{2.11}$$

In equation 2.11, P_f is the friction loss. The angular velocity of the turbine and the negative friction torque permit to estimate it:

$$P_f = Q_f \Omega \tag{2.12}$$

All the previous formulas come from the experimental methodology of Jooss [2022] and Bastankhah and Porté-Agel [2017] experiments. Indeed the current experiments use the same methodology.

2.2.2 Savonius wind turbine

In figure 2.6 it's possible to see different kind of VAWT. The first one on the left side is a Savonius without end plate on the top and the lasts are two models of Darrieus. The basic difference between Savonius and Darrieus consists in aerodynamic principle which permits the rotation of the turbine. Indeed Darrieus is mainly lift-driven turbine instead the Savoniuse turbine is drag-driven.

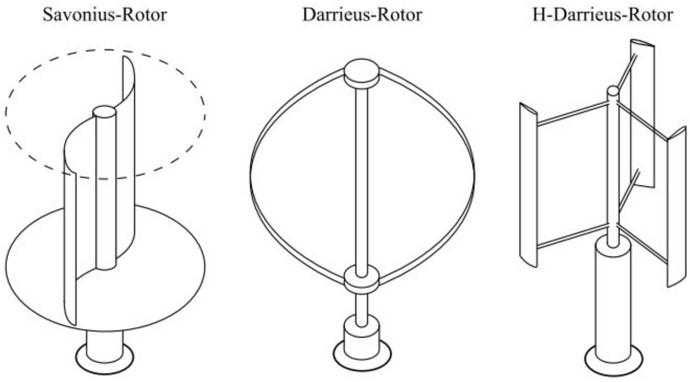

Figure 2.6: Different types of VAWT, figure from Schaffarczyk [2020]

The Savonius-style turbine is designed by cutting a cylinder into halves, along its central axis and replacing the semi-cylindrical surfaces sideways. Savonius, a Finnish engineer, invented this type of wind turbine in the 1920s, Abraham [2014]. Wind drag exerts force between the convex and concave portions of the blades and this is the reason why the rotor spin. However, at different rotational angular positions, lift force also contributes to the production of power. The advantages of this turbine are, Akwa et al. [2012]:

- low noise and angular velocity during operation;
- simple construction at low cost;
- acceptance of wind from any direction;
- many rotor configurations;
- high static and dynamic moment.

Figure 2.7 shows different forms of flow patterns, around the turbine blades during the entire rotational cycle of Savonius-style turbine, Abraham [2014]. These flow patterns are: free stream, coanda-type, overlap, separation, stagnation and vortex flows.

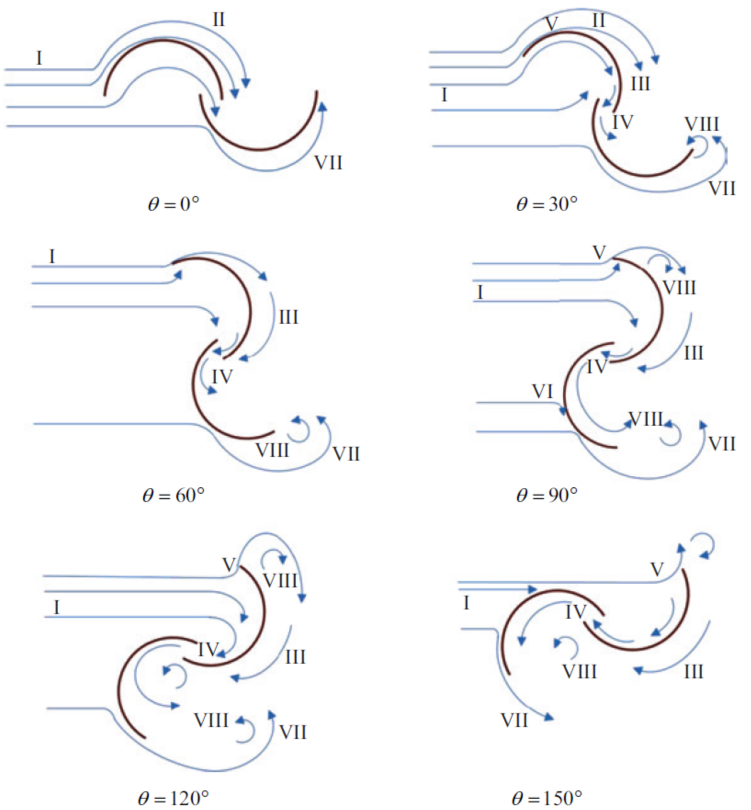

Figure 2.7: Flow around Savonius wind turbine, figure from Abraham [2014]

In particular, it can be seen from figure 2.7 that the flow around the Savionius turbine varies throughout its rotational cycles. Each Roman numeral in the figure represents a different flow pattern. The free-stream (I) can always be observed from the left side of the turbine. Like it's clearly visible at $\theta = 0°$ when the flow (I) reaches the turbine it adhers to the convex bucket of the turbine and it generates lift force. The tendency of the fluid to stay attached to the convex part of the Savonius reminds the Coanda effect, for this reason the name of (II) is Coanda flow. Figure 2.7 shows much more kinds of flows. For example at $\theta = 90°$ it is possible to see the vortex (VIII) generated by the separation of the flow (V) at the tip blade. It can be observed also the dragging flow (III) that it's an evolution of (II). The flow (III) together with (IV) help to restore the pressure drag on the convex side of the turbine and they contribute to generate power. At the intersection of the two buckets, in the center of the turbine, there is an overlapping flow (IV). In the end at $\theta = 90°$, the figure shows other two flows: the stagnation flow (VI) and the returning flow (VII). The lasts two flows don't contribute to an enhancement of the power of the rotor.

The aerodynamic study of Savonius VAWT is out of the topic of this thesis but it's possible to go deeply inside with Abraham [2014]. It can be found other descriptions of the flow around the Savonius in: Paraschivoiu [2002], Kang et al. [2014] and Pan et al. [2022].

Chapter 3

Methods

3.1 Wind Tunnel

The research was conducted in a wind tunnel, figure 3.1, located at the Energy and Process Engineering Department (EPT) of the Norwegian University of Science and Technology (NTNU) in Trondheim.

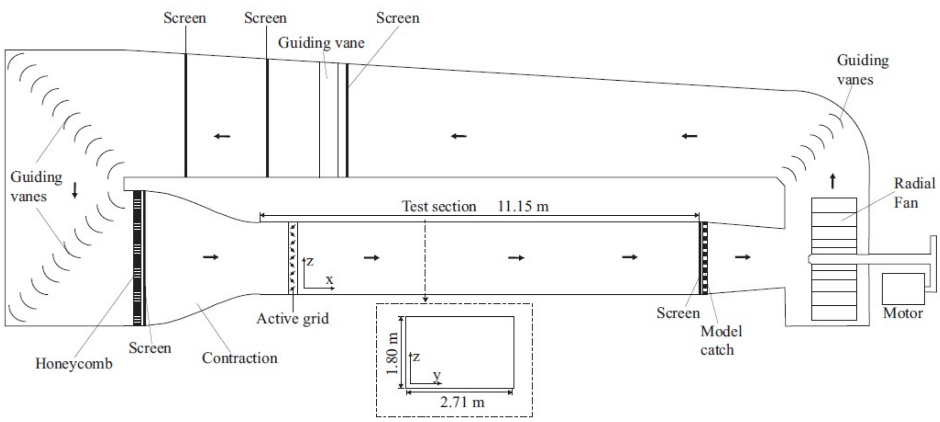

Figure 3.1: Scheme of wind tunnel at NTNU, figure from Jooss [2022]

The wind tunnel is closed loop and recirculating, with a test section that measures 11.15 meters in length, 2.71 meters in width, and 1.80 meters in height. A 220 kW radial fan located downstream of the test section powers the wind tunnel. It can be controlled by a variable frequency drive to regulate the flow velocity in the test section. The maximum velocity achievable in the test section is 23 meters per second. To ensure good flow quality, the flow passes through guiding vanes, screens, and a honeycomb. They make the flow homogeneous, isotropic, and with low turbulence inflow. The wind tunnel can be fitted with an active grid (like is possible to see in 3.1) that enables the control and adjustment of turbulence. The velocity of the flow in the test section is $9.05 m/s$, with a variation of 0.05 m/s. Monitoring the air parameters (such as pressure and temperature) it is possible to ensure the stability of the velocity during all the experiment. Indeed in the test section of the wind tunnel there is a thermocouple and the static pressure is measured manually with a barometer. Hence, in every moment it is possible to control that the free stream velocity is the correct one. The freestream turbulence intensity of the wind tunnel is less than 2%. It is necessary to say that the wind tunnel has been undergone minor changes since Jooss et al. [2022b] conducted the experiments so that may have caused slight variations in the results. To avoid any interference between the flow field of the experiment and the boundary layer of the wind tunnel, the experiments are conducted on an artificial floor, rather than directly on the test section floor. A large acrylic plate with a diameter of 1.4 meters and a thickness of 1 cm supports the model buildings, and four Alu-Flex legs with a height of 60 cm hold the plate in place. The edge of the plate is angled at 15 degrees to prevent flow separation. Additionally on the plate there is a small metal wire with a diameter of 2 mm placed 20 cm away from the edge. The wire induces a transition point of the flow in front of the model buildings.

3.2 Building and turbine models

The material of the two square cylinder model buildings is Ebaboard 0600. This material is usually used for creating models and it is easy to work. The laboratory technicians build the models using a CNC machine and specific CAD models. The square cylinders are $h = 20cm$ in height and $s = 10cm$ in width, with sharp edges, and one of the buildings has holes with a diameter of 9 mm on top for positioning the small Savonius wind turbines. Indeed, there are six different positions for the turbine in the streamwise direction. The turbine test positions are exactly at $0.15x/s$, $0.5x/s$ and $0.85x/s$ from the leading edge of both the buildings. The reference system used for the models places the X-Y plane parallel to the roof and the Z axis perpendicular to it, see fig 3.2. The main difference between these experiments and the previous study of Jooss et al. [2022b] is the height of the square cylinders. The current experiments aim to analyze the impact of higher models on turbine performance, with a height ratio that falls within a realistic range for urban wind turbines. Jooss et al. [2022b] state that a value between $0.13 \leq h_t/h \leq 1.03$ is common for two-storey buildings and a value between $0.08 \leq h_t/h \leq 0.62$ is common for three-storey buildings. Jooss et al. [2022b] chose $h_t/h = 0.3$. In the current experiments the ratio is $h_t/h = 0.15$. It means that the ratio is still inside the real range dimensions of urban wind turbine on multy-storey buildings but it is smaller than Jooss et al. [2022b]. With the building width s it's possible to calculate a specific Reynolds, formula 3.1, characteristic of the experiments and based on the flow parameters (velocity of the flow, density and dynamic viscosity):

$$Re_s = \frac{\rho U_\infty s}{\mu} \approx 60000 \tag{3.1}$$

One of the models is internally empty to allow the installation of a support system for the torque motor and infrared sensor necessary for determining turbine performance. This support system is 3D printed at the laboratory with PLA material and includes vanes for the measurement instruments. The square buildings are in tandem configuration on the plate at a distance of $2s$ in order to compare the experiments with Jooss et al. [2022b], figure 3.2. The windward building is at a distance of $5s$ from the leading edge of the artificial plate.

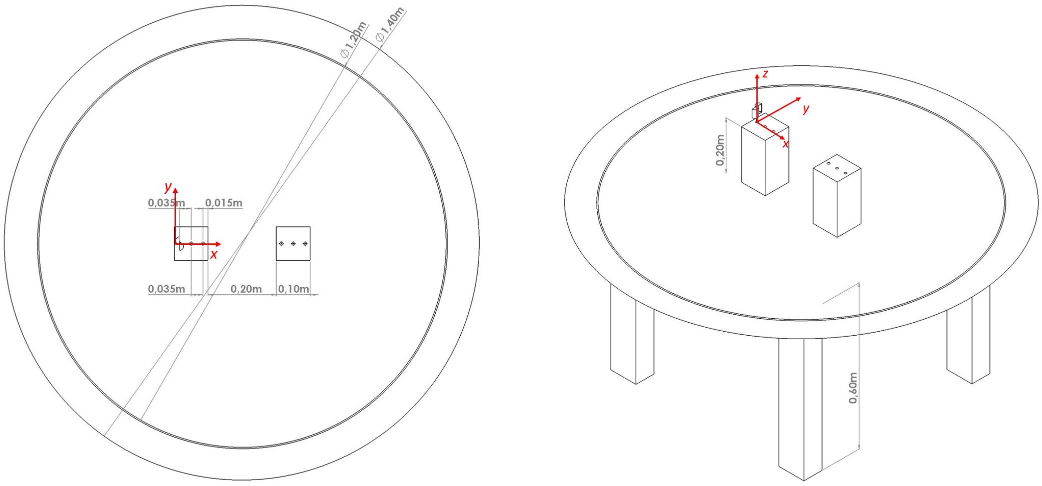

(a) Top view (b) Isometric view

Figure 3.2: Setup in the test section

Other important consideration could be done relatively to the design of the small wind turbine. The design of the turbine is the same of Jooss et al. [2022b] and it consist on a two-bucket Savonius turbine 3.3. It has a diameter of $d_t = 0.4s$ and the height of the rotor area is $h_t = 0.3s$. The two buckets are overlapped of 0.05s. The overlapping permits a less contrast torque during the starting. The Reynolds number of the turbine (based on the diameter of the turbine d_t) is approximately 24 000.

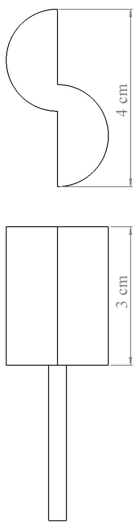

Figure 3.3: Model of Savonius turbine

The turbine has two configurations (Low and High) with distances of +0.08s and +0.16s from the roof to the lower edge of the rotor swept area. Indeed the centers of the rotor swept area are respectively placed at 0.23h and 0.31h above the roof. The turbine is 3D printed with PLA (polylactide acid) material with high resolution of the filament in all the directions. The 3D printed realization of the turbine has lot of advantages related to the time of the realization of the model and its replicability. However, the small size and material properties of the PLA turbine made it somewhat fragile and required careful handling during the experiments. Moreover the elastic module (E) of the PLA material is not so high and it is the reason why during the experiments the shaft of the turbine shows a little of bending. Another weakness of the turbine is the junction between the rotor shaft and engine torque, where it is difficult to ensure perfect adherence between the two components.

3.3 Measurements

3.3.1 Cobra and Pitot probes: flow measurements

The pitot measures the flow velocity in the freestream. The Pitot probe is a well-known instrument that permit to calculate velocity of the flow by difference of total and static pressure. In the experiment the probe was connected to a pressure transducer with the K constant of 62.58 Pa/Volt and the last one is connected to a digital data system acquisition. The acquisition time is 10 seconds and the frequency of sampling is 100hz. Another kind of probe is used for the measurements of the flow around the buildings and for determining the flow field on the plate without the models. It is a multi-hole probe, also called 'Cobra Probe' produced by Turbulent Flow Instrumentation (TFI), see fig 3.4. It can measure three components of the velocity field. The Cobra Probe has a head with multiple faces, and it contains four pressure taps that are 0.5 mm in size. The taps are connected, through tubes, to pressure transducers located in the body of the probe. The probe is useful for time-averaged measurements of the flow (like the disc's boundary layer) but also for turbulent measurements in real time (like the turbulence intensity I_{uu}, defined in 2.5). The acquisition frequency of the probe is 2048Hz and the sampling time is 30s. The probe uncertainties is $\pm 0.5 m/s$.

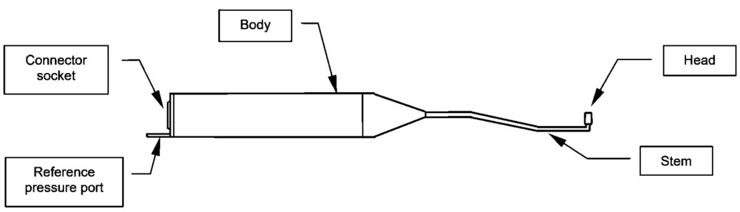

Figure 3.4: Cobra probe

Disc's boundary layer

The flow field over the plate where the two model buildings are located is the first item analysed with the Cobra probe, as shown in figure 3.5. Intially, the boundary layer was measured over the disc, at $x/s = 0$ (see S.R. in figure 3.2), and the measurements were taken without the two buildings in the middle.

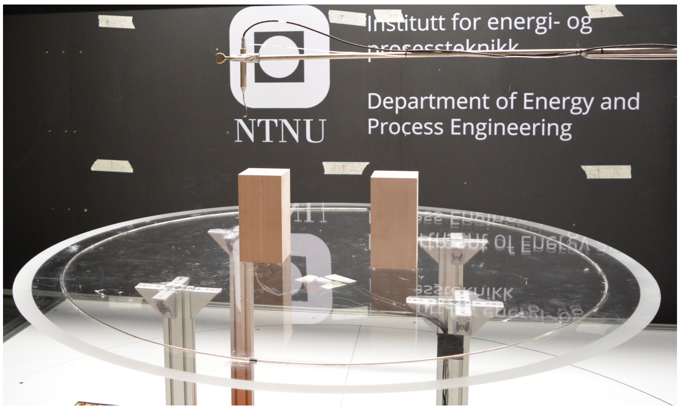

Figure 3.5: Flow measurements around buildings

Figure 3.6 shows the adimensionalized boundary layer. In this instance, the boundary layer is around 2.2 cm thick. Therefore, the buildings are partially submerged in the disc's boundary layer. Through the measurements of the flow on the disc it has been calculated the displacement thickness δ^*, the momentum thickness θ and the shape factor H of the boundary layer:

$$\delta^* = \int_0^\infty \left(1 - \frac{u}{U_\infty}\right) dz \tag{3.2}$$

$$\theta = \int_0^\infty \frac{u}{U_\infty} \cdot \left(1 - \frac{u}{U_\infty}\right) dz \tag{3.3}$$

$$H = \frac{\delta^*}{\theta} \tag{3.4}$$

The shape factor H is a common parameter of the integral analysis of the boundary layer and it permits to understand if it is turbulent or laminar. According to the theory an H value $\approx 1.3 - 1.4$ is associated to a turbulent boundary layer while an H ≈ 2.6 indicates a laminar boundary layer. The values of δ^* and θ of the current boundary layer are respectively: $2.06mm^2/s$ and $1.73mm^2/s$. Their ratio gives a shape factor H ≈ 1.3. So, it is possible to say that the boundary layer is turbulent.

3.3.2 Arduino, InaSensor and Engine: power measurements

The most important measurement for determining the performance of the turbine is the coefficient of power together with the tip speed ratio, fundamental to define the Cp-TSR

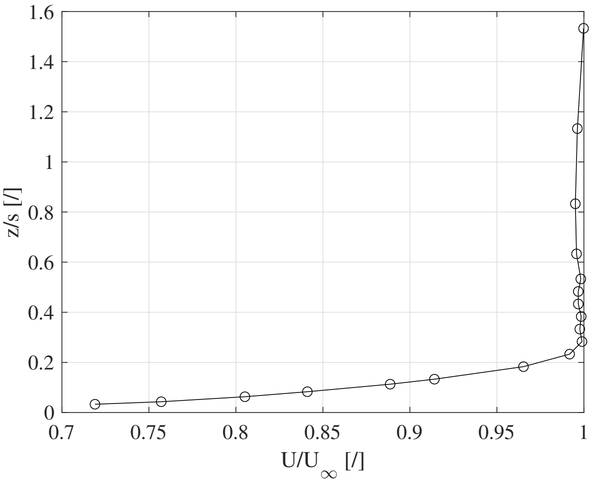

Figure 3.6: BL on plate at x/s=-0.5

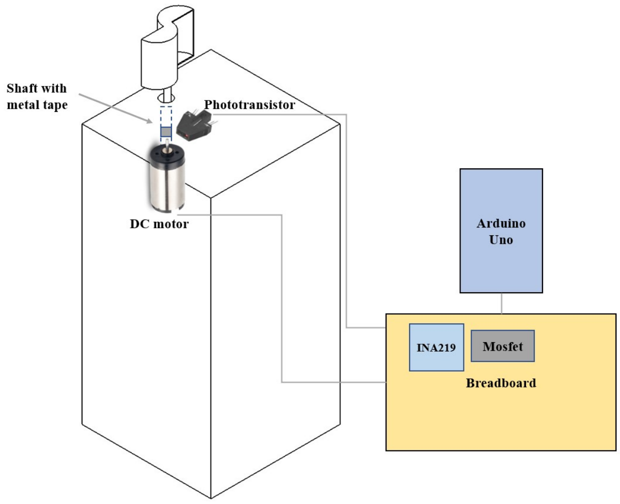

Figure 3.7: Setup for measuring power

curve. The acquisition of the data is performed using the setup of Jooss et al. [2022b]. In figure 3.7 it is possible to see a scheme of the measurement circuit.

Like it is stated in equation 2.11, the mechanical power is the sum of converted power and friction losses. The friction power is estimated and the converted power is calculated thanks the data acquired by the measuring system. The components of the measuring system are:

- 12G88 Athlonix (brushed DC motor);
- INA219 High Side DC (current sensor);
- OPB703/705 (reflective object sensor);

- IRF540NPbF (mosfet).

A micro controller (Arduino Uno) connect all the components. The current sensor and the DC motor work together, indeed the electricity produced by 12G88 Athlonix (directly connected to the rotor shaft of the turbine) is sampled by the INA sensor. So thanks to the coefficient $k_t = 4.9mNm/A$, inserted in the formula 2.10, the electromagnetic torque is easily estimated. The phototransistor is close to the shaft of the turbine where a metal tape is attached. This sensor can read the rounds per minute performed by the turbine, so the angular velocity. At this point knowing the electromagnetic torque and the angular velocity of the turbine, using formula 2.9, it is easy to calculate the converted power. The last element is the high frequency mosfet. It opens and close the circuit that control the DC motor and so acting on it is possible to acquire different point of the CP-TSR curve. A script which acts on Arduino Uno controls all the variables acting in the circuit, like the duty cycle of the mosfet or the acquisition time.

3.4 Error analysis

In order to perform an error analysis of the power coefficient and the tip speed ratio it's necessary to use the law of error propagation 3.5, of Wheeler [1996]:

$$\frac{\delta_F}{F} = \sqrt{\left(a\frac{\delta_1}{x_1}\right)^2 + \left(b\frac{\delta_2}{x_2}\right)^2 + .. + \left(N\frac{\delta_n}{x_n}\right)^2} \tag{3.5}$$

In formula 3.5, F is the function that depend on several variables : $F = x_1^a x_2^b ... x_n^N$. δ_f represents the error of the function and $\delta_1/x_1 ... \delta_n/x_n$ are the relative errors (random and biased errors). In the previous formula are not considered the correlation terms because it is supposed that each variable is independent.When dealing with measurements of variables like Cp and λ which depend on multiple factors, it is important to use the law of error propagation to account for the effects of both random and systematic errors. The formula for error propagation consent to estimate the overall uncertainty in measurements by considering how errors in each contributing factor affect the final result. To calculate the uncertainty for Cp and λ, it is necessary to determine the individual contributions of both random and bias errors for each variable involved.

The variables affected by errors in the Cp equation 2.6 are: free stream velocity, density (calculated with the ideal gas law), rotor area, and mechanical power (see 2.11). The Pitot probe has a bias error of 0.5% and it's relative calibrator manometer has an error of 0.1%. In case of the density it's possible to define the systematic error of the related measured temperature and pressure which are respectively: 0.075% and 0.01%. In the previous cases the error analysis doesn't account the random errors of the variables, indeed they are negligible. The error related to the measure of the rotor area is not taken in account because of the high definition of 3D Printer.

Other important sourch of error in formula 2.6 is the mechanical power P_m. Indeed the current and the angular velocity measurements inside P_c of the formula 2.11 have bias and random errors. The random errors are estimated with a long acquisition (around 10 minutes). The random errors of the current and the RPM are respectively: 0.5% and

7.68%. The last value is relevant and it affects significatively the final error of the Cp and TSR. The manufacturers provide the systematic errors for the current and the angular velocity: 0.5% and 0.04%. With all the previous values of relative error is possible to calculate, through 3.5, the errors for Cp and TSR, respectively: 8.5% and 8.1%. The last values are higher than the previous experiments (Jooss et al. [2022b]) and like it is stated previously it's due to some instabilities with the acquisition of the angular velocities.

Chapter 4

Results and discussion

4.1 Flow field

Understanding the location of the point of stagnation in front of the windward building is crucial before focusing on the building's top. To determine the location of the stagnation point, it's possible to referring to figure 4.1 which shows the velocity component in Z direction w in front of the model, at $x/s = -0.1$. The graph indicates that the velocity becomes negative around 7.5 cm from the disc's floor. The low height of the stagnation point let us comprehend how the w velocity may significantly increase before it reached the top edge of the building, raising and providing more energy to the recirculation zone on top of the model building. Additionally, the graph shows that the vertical flow slows down as it moves from the roof of the building to the free stream flow, which has a positive effect on the rotation of the turbine. Differently in the flow field that is possible to observe in a prior study (Jooss et al. [2022a]), in the current experiment the location of the stagnation point is lower than half of the height of the building.

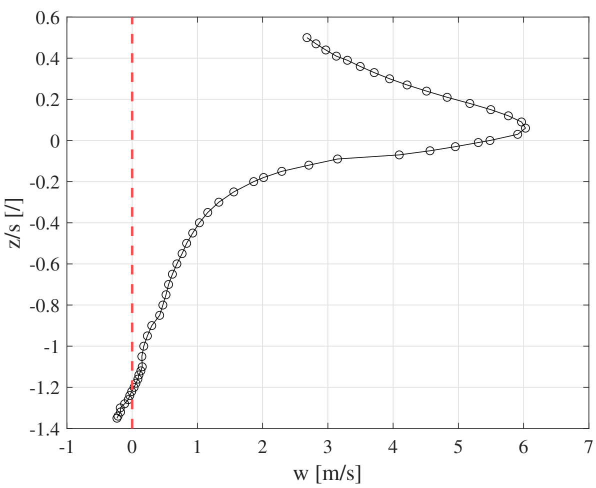

Figure 4.1: W component in front of windward building

The figure 4.2 is crucial for understanding the height of the velocity profile over the top of the windward building. The figure shows the results of three different positions, each corresponding to the placement of the turbine. It can be seen that the velocity profile increases as one moves from the front of the building towards the back. Specifically, the velocity profile reaches the free stream velocity approximately at $z = 1.7cm$ on the front position, at $z = 3.6cm$ on the central position, and $z = 4.5cm$ on the back. It means that, depending on the height configuration of the turbine (whether it is low or high), the turbine could be completely immersed or not within the recirculation zone. The current velocity profiles are in agreement with the results found in other studies, like Jooss et al. [2022a].

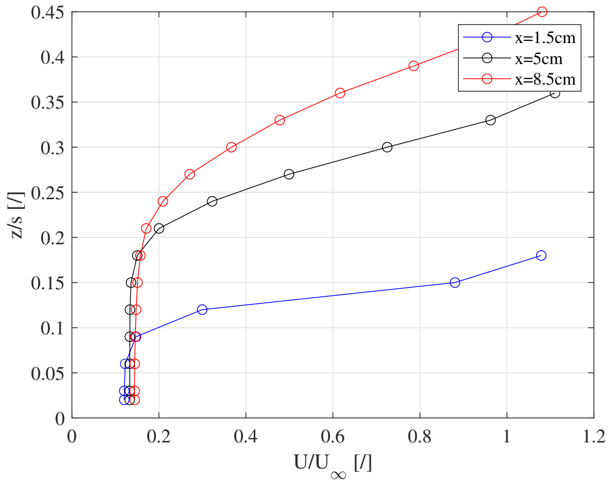

Figure 4.2: Velocities profiles on windward building

The flow field over the leeward building can be seen in graph 4.3. In this case, the flow that separates from the windward building's back it attaches to the leeward building's front. In this instance, the velocity of the flow close to the roof of the building is larger than those on the windward model. The shape of the velocity profile is less steep and the free-stream velocity is reached at about $z/s = 0.5$. In the last graph, it is also clear that velocity increases as one moves from the front to the back of the square cylinder roof, which is advantageous when the turbine is positioned last.

An overview of the flow field above the windward building may be seen in the velocity vectors plot of figure 4.4. In the X-Z plane, this graph displays the velocity vectors made up of the u and w components. The vectors are in accordance with the ratio between the u component and the u_∞, as indicated in the legend above the figure. The colors show some relevant flow informations: primarily an acceleration zone similar to what might be seen in Jooss et al. [2022a]. In particular the blue vectors identify the decellerated flow on the roof, with a range value of $0 < U/U_\infty < 0.99$, this ratio range reminds the definition of the upper edge of the boundary layer on different aerodynamics bodies. Red and green vectors represent the transition between decelerated and accelerated flow, as shown by Jooss et al. [2022a]. At the end the yellow vectors display the increment of

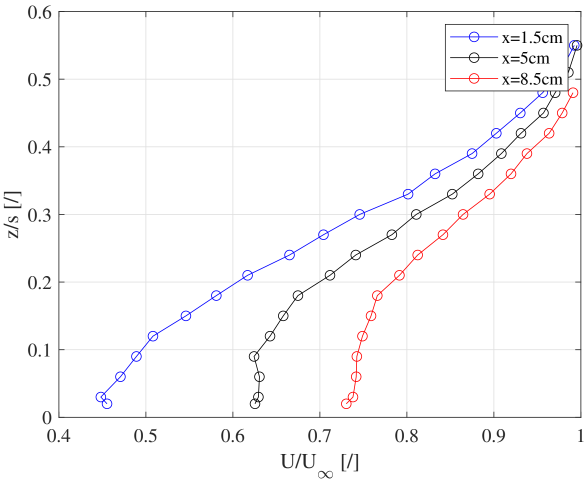

Figure 4.3: Velocities profiles on leeward building

velocity ($> 1.1U/U_\infty$) over the recirculation zone. It is also put in evidence the three positions on the buildings where are placed the turbine at $x/s = 0.15$, $x/s = 0.5$, and $x/s = 0.85$. There are also two different lines for the configuration of the turbine: the dot line represents the turbine placed 8 mm over the roof and the continue line represents the one at 16 mm over the roof. Like it's possible to see in the frontal and central positions the turbine can benefit of a good flow, especially for the first. Indeed, for the high and low turbines on the windward building, almost all the vectors are red and it means that the turbines can benefit of velocities which are equal or little higher than the free stream velocity. In the central position the velocity is not so good especially for the low turbine where the reverse flow affects the flow field. Here the cobra probe is completely inside the recirculation zone put in evidence by Jooss et al. [2022a] and it's difficult to say too much about the flow. Indeed, the cobra probe can't acquire the velocity from the back but the drastic reduction of the magnitude of the vectors could be the explanation. In this postion the turbine can generate a lot of power only if it is placed at a high location due to the strong magnitude of the flow vectors. At half height of the turbine, the flow is within the recirculation zone and it does not contribute much to the power generated by the turbine. However, beyond this zone, there are yellow vectors which indicate an accelerated flow that contributes greatly to the available power. The acceleration zone is advantageous and it extends between 3.7 cm to 5 cm in the central position and between 4.3 cm to 8 cm in the back position. Although it would be ideal to take advantage of this high velocity zone, it is not feasible due to the distance from the roof and the potential for high bending of the turbine axis and stress on the roof. In the back position, due to the low magnitude velocity vectors the low turbine does not spin in this location as it is fully within the recirculation zone. Inside the area that represents the high turbine the flow is mainly slow. However the turbine can gain a little of speed from the accelerated zone on its top. For this reason in this position the high turbine can at least spin.

The figure 4.5 displays a velocity vectors graph of the flow field in the X-Z plane on the

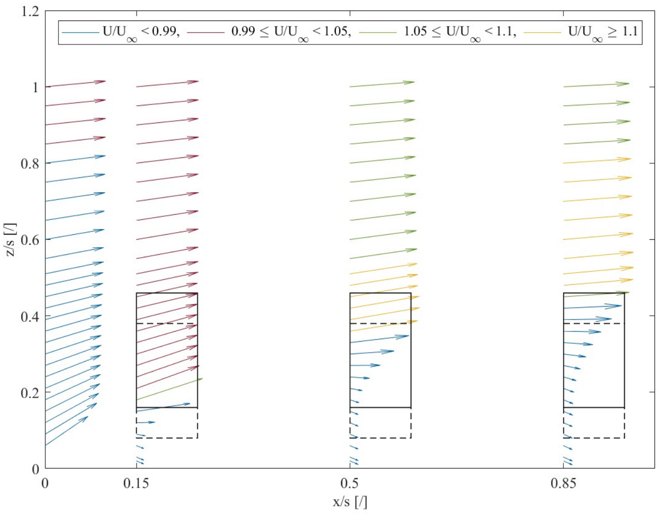

Figure 4.4: Flow field over windward building

leeward building. In this case, there are only two different colors of vectors as the range of flow magnitude variability is smaller than on the windward building. On the front edge of the building, the vectors are skewed towards the roof due to the flow reattaching after the separation at the back of the windward building. As result, a recirculation zone is not present and the flow tends to accelerate towards the back, allowing the turbine to generate more power in the back position compared to the frontal position. Similar to the graph 4.4, the flow velocity tends to decelerate near the wall and accelerate towards the free stream as it moves away from the wall. In general, the turbine can spin in any position or configuration, but the velocity magnitude of the vectors is lower, resulting in less available power.

Figure 4.6 shows the turbulence profiles of the u component of velocity I_{uu} on the Z direction on the top of both the models buildings. The graphs are important because the turbulence can affect the performance of the turbine. In particular, in 4.6a (on the windward building) it's possible to see that going towards the back of the building, the turbulence increases because the recirculation zone become larger. Especially, in the front position the turbulence profile is narrow and reach a maximum of 30% instead in the other two positions the peaks of turbulence are around 40%. In central and back positions also the values of the turbulence intensity averaged over the height of the turbine is higher compared to the one on the first position. Indeed, the values are : 10.77 %, 21.91% and 25.46% (for low configuration of turbine, from position 1 to 3) and 2.86%, 18.36% and 23.88% (for high configuration of turbine). These data explain also the worst performance on the central and back positions. Like it's reported in KC et al. [2019] the turbulence of the flow can negatively affect the performance of the VAWT and it has also lot of impact on fatigue loading. Figure 4.6b shows the turbulence profiles on the leeward model building at different locations. The profiles at positions 4, 5 and 6 are completely dissimilar from the previous ones. In this case the highest value of the turbulence is on the

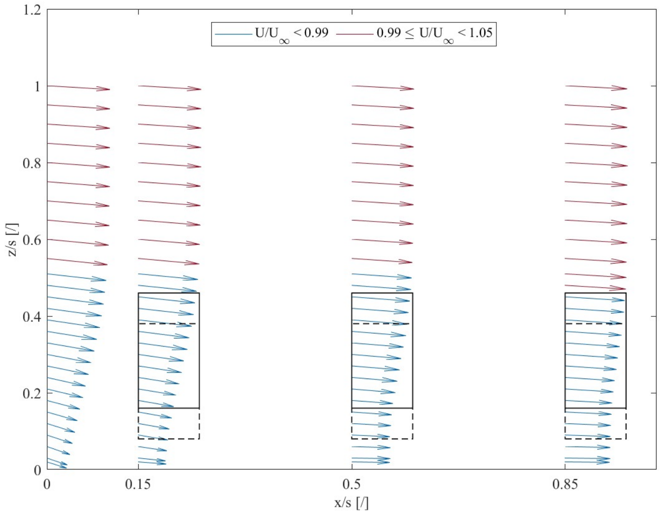

Figure 4.5: Flow field over leeward building

first position, close to the leading edge of the model, where the flow try to reattach after the separation from the windward building. The turbulence profiles here are also different from the ones on figure 4.6a because they are thicker close to the roof and turbulence deacreses towards the freestream. The highest value of the turbulence on the leeward building is lower than on windward building for each positions but it remains constant for a larger area along the Z profile.

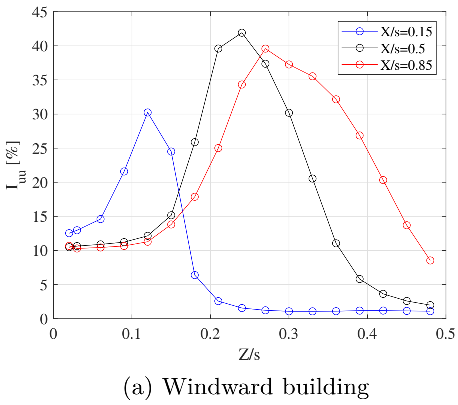

(a) Windward building

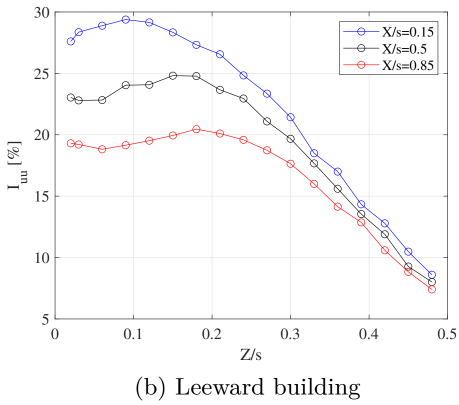

(b) Leeward building

Figure 4.6: Turbulence profiles

At the end it is possible to see the flow field in the ZY plane in order to understand how it evolves across the rotor area of the turbine. In figure 4.7 there are different graphs and they show the different behaviour of the flow between windward and leeward buildings. Watching the positions 1, 2 and 3 on the windward building it can be said that the flow close to the roof (until $z/s = 0.12$) tends to slow down going towards the lateral edge. Considering the flow at higher positions (from $z/s = 0.18$ to $z/s = 0.48$) it is clear that the flow is not affected significative in velocity changes. On the leeward building the behaviour of the flow is different. Indeed, the velocity on that building, at each positions, tends to increase going towards $y/s = 0.2$. In the last case the turbine can benefit of this raise of velocity.

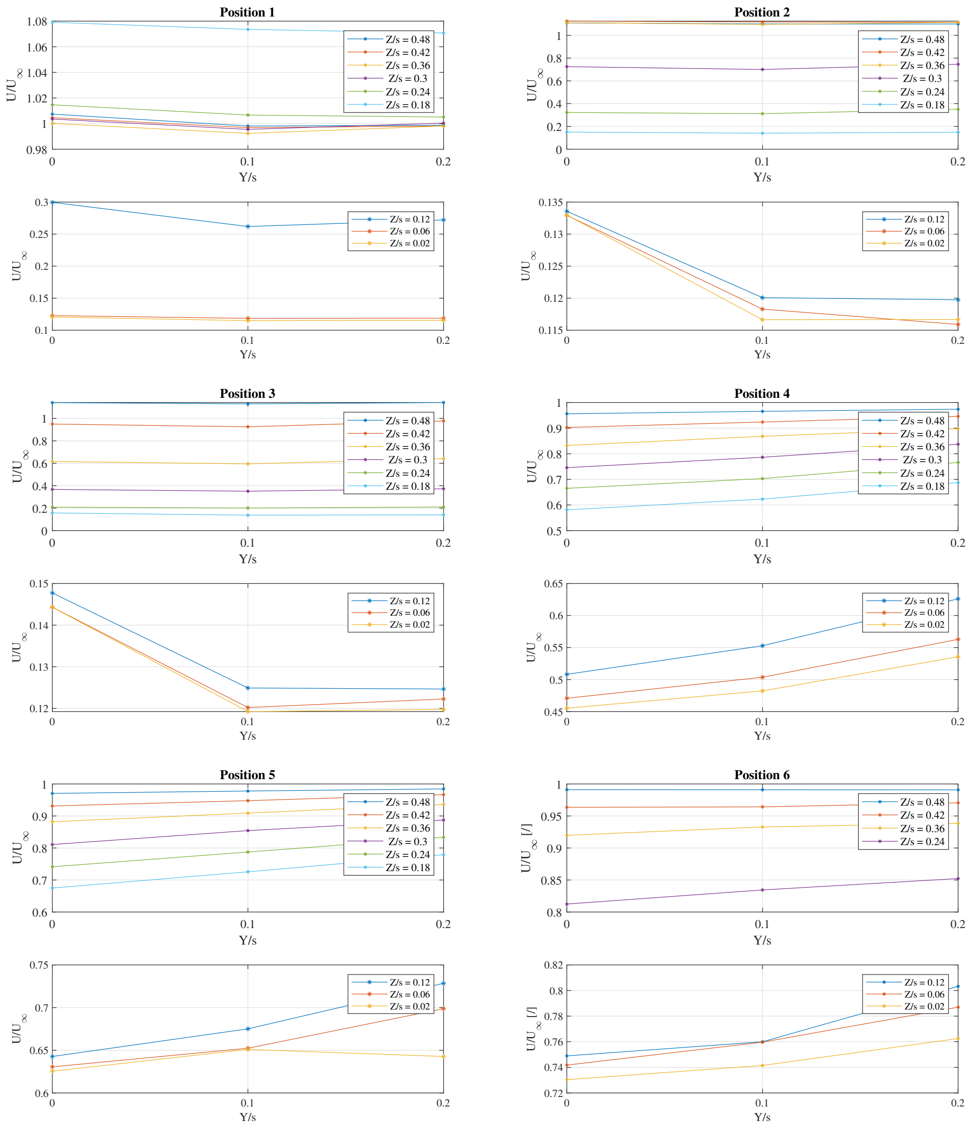

Figure 4.7: Z-Y plane flow field

4.2 Power curves

After examining the flow field on top of the buildings, it is easier to understand the behavior of the turbine in different positions. Next, the results of the Cp-TSR curves are presented. It's important to note the positions of the turbine in figure 4.8, each of which corresponds to two different configurations, low and high. Before analyzing the effect of position on the power curves, it is important to examine the reference curve obtained without a building in the current experiments' freestream. In figure 4.9, the

Figure 4.8: Turbine positions on top of the buildings

black curve represents the current experiment, while the other represents reference Jooss et al. [2022b]. The Cp values observed in the curves are low because the Reynolds number of the experiments is small. Indeed the $Re_{dt} = 24000$ based on the diameter of the turbine affects the rotor performances. Like it's stated in Akwa et al. [2012] the maximum Cp of the turbine decreases as the Reynolds number decreases. An attempt was made to reproduce the conditions of Jooss et al. [2022b] for comparison purposes. Of course, every experiment is unique, and perfect replication is impossible. Figure 4.9 shows the power curve with the error bars. As can be seen, the error in the new experiments is larger than in Jooss et al. [2022b] due to certain reasons, like it is stated in section 3.4. The new error of Cp is about 8.4%, while the previous one was approximately 3.5%. However the shape of the curves is similar, the error bars intersect at each point and the maximum Cp is almost the same (the new one is 7.14% higher). In absolute value the $Cp_{0,max}$ of the current experiment is 0.045 and in Jooss et al. [2022b] it was 0.042. Thus, it is reasonable to compare the experiments.

At this point it is possible to see the results of the curves at each different positions and configurations and later in the next section 4.3 it will be possible to see the comparison with Jooss et al. [2022b]. Starting from the figure 4.10a there are three different Cp-TSR curves related to high turbines. It's clearly visible that the curve in the front position has the highest value of Cp compared to the central and back curves. It has the highest Cp_{max} also compared to the reference curve so it means that the turbine can benefit of accelerated flow, indeed the Cp_{max} is 2.2% higher than $Cp_{0,max}$. The last curve has also a large interval of TSR with high Cp so it could be useful for different wind speeds, between 0.32 and 0.46 of λ. Another parameter that explains the good result from the turbine in

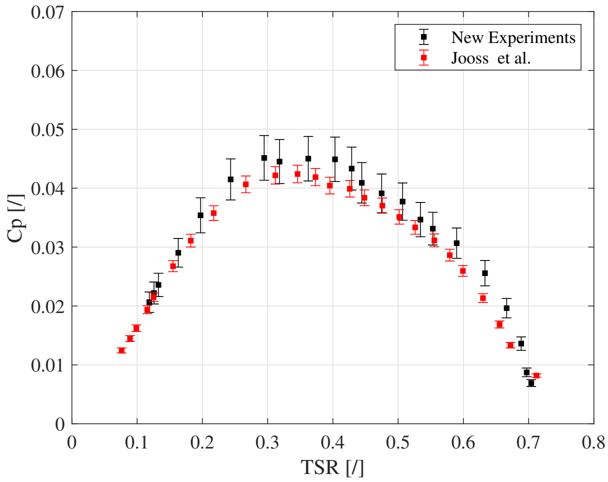

Figure 4.9: Cp-tsr reference curve

front position is the turbulence profile in that place, here indeed the turbulence reaches the lowest peak and it is not distributed along all the height of the turbine. The Cp-TSR curve for the central position is similar to the previous one for low TSR, but as the TSR increases, the curve does not reach the same maximum Cp as the front turbine. Lower Cp_{max}, about 21.7% less than the frontal could be explained by higher turbulence profile (here the peak is over 40%) and the reverse flow inside the recirculation zone. Indeed, this turbine can benefit of a small part of acceleration zone on its top but there is also a big part of slowed flow on the low part of the wetted area of the turbine. The result for the turbine in the back position is the worst compared to the central and front positions, with a maximum Cp of 0.01. The turbine in this position is located entirely within the recirculation zone and it experiences high turbulence.

In the figure 4.10b it's possible to see the Cp-TSR curves for the low turbines on windward building. In this configuration there are only two curves (frontal and central positions). Indeed, the turbine in back position is affected by a very low inflow velocity because there is an high component of reverse flow generated in the recirculation zone. It is the reason why the turbine in the third position doesn't spin. Another important result for positions 1 and 2 is that the curves are smoothly compared to the high turbine and they have a bigger zones of Cp_{max}. In both cases the Cp_{max} is lower than high turbines in the same positions and it is due to the low velocities in the wetted area of the turbine, see figure 4.5. Indeed, in the frontal position the turbine reaches a Cp_{max} of 0.03 and in the central position it is 0.014.

In figure 4.11, the analysis of the results continues by examining the power curves on the leeward building. In this situation, the trend is different, indeed the turbine reaches the maximum power coefficient as it moves towards the back of the building. As shown in figure 4.6, it can be seen that the flow reattaches to the top of the building after separating from the first structure, resulting in higher velocities towards the rear of the roof. In particular, on figure 4.11a, it is possible to observe the curves for different

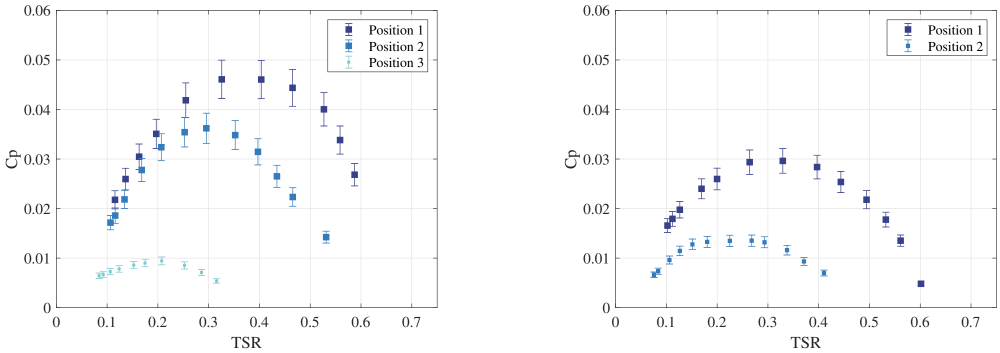

(a) High turbine (b) Low turbine

Figure 4.10: Cp-Tsr curve on windward building

positions of high turbine configuration. The turbine achives the best Cp within a range of 0.2 to 0.3 TSR in all the positions. The curve of position 6 reaches the highest value of Cp_{max}. It is noteworthy that the highest Cp reached from all three curves is lower than the Cp on the windward building in the same positions. The curves at positions 6 and 5 are almost overlapped because the difference in flow velocity in this location is minimal. On the other hand, the curve from the turbine in position 4 is relatively low because near the front edge of the building, the flow reattaches and slows down. Comparing figure 4.10a with 4.11a it's possible to see that especially for the frontal and central turbine, on the windward building the turbine reaches the highest Cp at high TSR. Examining graph 4.11b, there are curves for low turbines on the leeward building. In this case, the differences between low and high turbines, as seen in figures 4.11a and 4.11b , are not as pronounced as for the turbines on the windward building. There is a slight decrease in flow speed for the low turbine, but this does not have a significant effect on the power curve. For the low turbine on the leeward building there is a big difference between the curves of positions 5 and 6 and the curve of position 4.

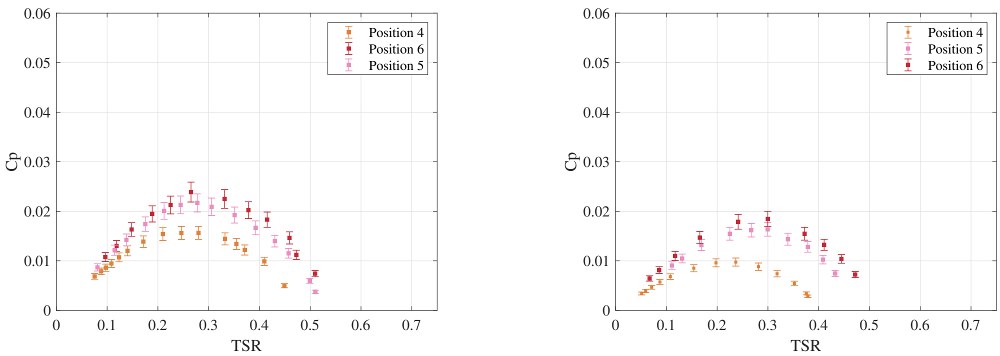

(a) High turbine (b) Low turbine

Figure 4.11: Cp-Tsr curve on leeward building

Finally, in this section, figures 4.12 and 4.13 provide an analysis of the correlation between the available power on the buildings and the actual Cp_{max}. The definition of the coefficient of available power used in this analysis is:

$$Cp_a = \frac{\frac{1}{2}\rho\tilde{U}^3 A}{\frac{1}{2}\rho U_\infty^3 A} = \frac{\tilde{U}^3}{U_\infty^3} \tag{4.1}$$

Jooss et al. [2022a] used the coefficient for a similar analysis. In formula 4.1 the speed $\tilde{U}$ measured along the height of the turbine (for low and high configurations) is an integral average. This velocity is acquired with cobra probe and without wind turbine in the flow field. Like it's stated in Jooss et al. [2022a] the estimated power is less correlated with the real power. The results give a correlation coefficient $r(Cp_a, Cp_{real}) = cov(Cp_a, Cp_{real})/\sigma_{Cp_a}\sigma_{Cp_{real}} = 83.14\%$. Figures 4.12 and 4.13 show clearly how each positions is correlated with the estimated power on the windward and leeward building.

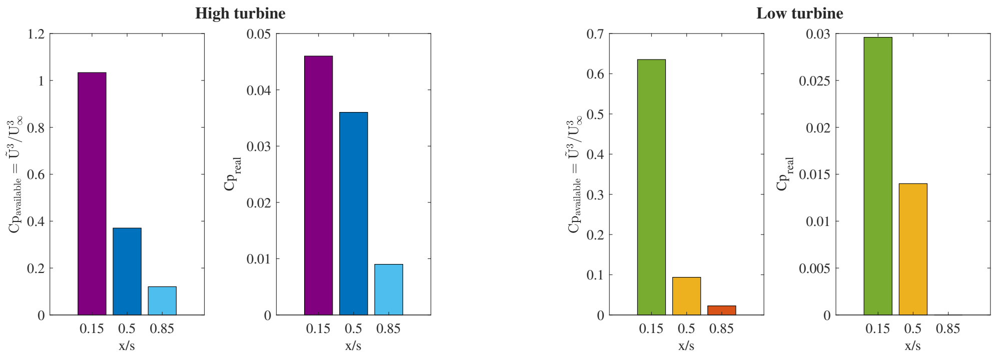

(a) High turbine analysis (b) Low turbine analysis

Figure 4.12: Coefficient of available power ($Cp_{available}$) and measured mechanical power (Cp_{real}) on windward building

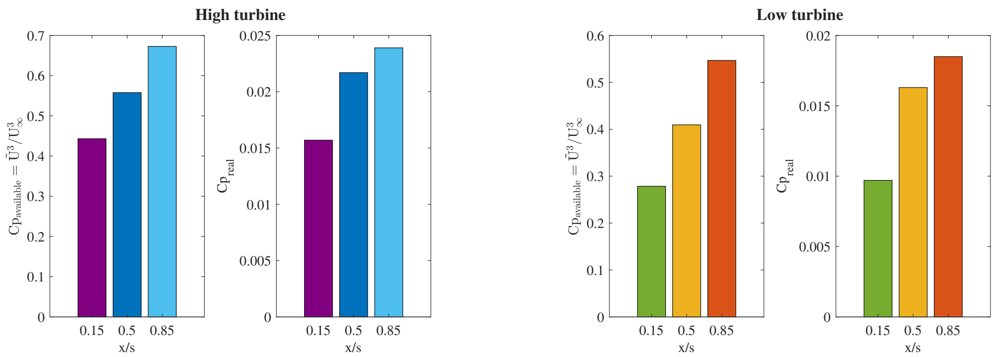

(a) High turbine analysis (b) Low turbine analysis

Figure 4.13: Coefficient of available power ($Cp_{available}$) and measured mechanical power (Cp_{real}) on leeward building

4.3 Comparison with similar experiments

In this section it's made an analysis comparing the results of this thesis and the results of Jooss et al. [2022b]. The setup of the current experiments is the same of Jooss et al. [2022b] but the model buildings are different. In the test section of the wind tunnel there is also the same free stream velocity that gives the same Reynolds $Re_{dt} \approx 24000$ and $Re_s \approx 60000$. Figure 4.14 shows the two different setups of the experiments on the circular plate. In 4.14a there are two square cylinder of height equal 20 cm and width of 10 cm, separated by a distance of 20 cm (two times the width) and this is referred to the current experiment. Figure 4.14b shows two cubes with edges of 10 cm Jooss et al. [2022b]. Before comparing the results of the Cp-TSR curves from the two different experiments it has been made an analysis of the flow field over the small cubes (at x=0, 2.5, 5, 7.5 and 10 cm) and also it has been reacquired power curves of some positions. Good agreement was shown between the current results and the data of the new ones experiments. So one of the first important results it's the velocities profile comparison in figure 4.15 between current and Jooss et al. [2022b] experiments.

(a) 20cm buildings (b) 10cm buildings

Figure 4.14: Current setup and Jooss et al. [2022b]

In figure 4.15, the distinct shape of the velocity profile on the windward building at x=5 cm is clearly visible. The taller building exhibits a larger velocity profile, indicating that the freestream velocity is nearly 3 mm above the height of the smaller building's velocity profile. As seen in figure 4.15, the velocity profile is the same for both the small and tall buildings until 1.5 cm above the roof. This variation in the two velocity profiles could be attributed to the high vertical component of the velocity in front of the building, as seen in figure 4.1, which can push up the recirculated and mixed turbulent flow over the square building.

Subsequently to the analysis of the flow field, in table 4.1 there is an overview of the most significative results from the experiment comparison, i.e. Cp_{max} and related Tip Speed Ratio. Specifically for high turbines on the windward building the results show that all the positions on ten-centimeter cube perform better than on twenty-centimeter square building. Only for the first position on the square cylinder is possible to reach a slightly higher Cp_{max}. Regarding the related TSR there are also slight differences, indeed in almost all the cases of turbines on higher buildings, the Cp_{max} is at low TSR. For low turbines, the same trend of differences is still evident on both the square-cylinders. The

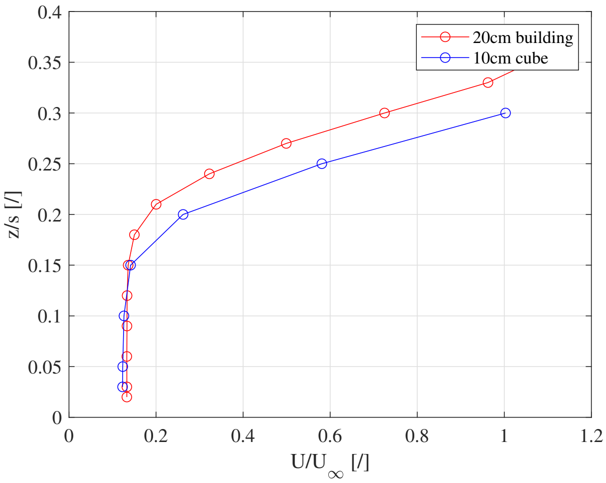

Figure 4.15: Velocity profile comparison on windward building at x = 5cm

main differences are at positions 1, 2, and 3 on the windward building. Indeed the flow in that postions is more affected by changes in height.

Table 4.1: Comparison Cp and TSR with Jooss et al. [2022b]

	New Experiments (20 cm buildings)				**Jooss et al. (10 cm cube)**			
	High		*Low*		*High*		*Low*	
Pos.	Cp max	Λ_{opt}	Cp max	Λ_{opt}	Cp max	Λ_{opt}	Cp max	Λ_{opt}
1	0.046	0.33	0.030	0.33	0.044	0.33	0.036	0.35
2	0.036	0.30	0.014	0.27	0.049	0.46	0.028	0.27
3	0.009	0.21	/	/	0.030	0.36	0.005	0.16
4	0.016	0.28	0.010	0.24	0.016	0.25	0.012	0.28
5	0.022	0.28	0.016	0.30	0.019	0.31	0.017	0.30
6	0.024	0.27	0.019	0.30	0.021	0.29	0.02	0.29

Referring to table 4.1 is possible to define the percentage variation between the Cp_{max} of the current experiments and Jooss et al. [2022b]:

Table 4.2: Percentage comparison of Cp_{max} with Jooss et al. [2022b]

Pos.	*High* $\frac{Cp_{max,20cm}-Cp_{max,10cm}}{Cp_{max,10cm}}$ *[%]*	*Low* $\frac{Cp_{max,20cm}-Cp_{max,10cm}}{Cp_{max,10cm}}$ *[%]*
1	3.9	-18.2
2	-25.7	-51.6

Table 4.2 continued from previous page

3	-68.0	/
4	0.4	-21.6
5	13.1	-0.7
6	15.2	-6.9

After a general overview, a comparison of power curves for different positions of the turbine can be found in detail.

Figure 4.16 shows the first position on the windward building for high and low turbines. The power curve for the new experiment in figure 4.16a appears to be slightly higher than the experiments in Jooss et al. [2022b], but it is important to take into account the larger error bar (8.5% for the coefficient of power Cp). In general, it can be said that the curves are nearly overlapping. In figure 4.16b there is a graph with the results of low turbines and here the new experiment on the higher building performs worse. The shape of the curves becomes quite different especially when the tip speed ratio is above 0.3.

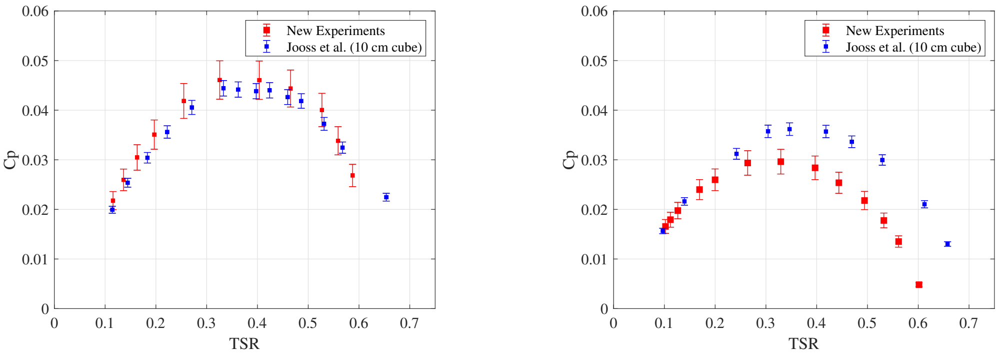

(a) High turbine

(b) Low turbine

Figure 4.16: Position 1

Results in figure 4.17a are similar to the previous ones, with low Cp at high TSR for the current experiment. In this case there is a huge difference at high TSR around 0.45, where the current Cp is 45% lower than the previous curve. In the other graph of figure 4.17, there are two completely different curves. The Cp-TSR curve for the new experiment does not reach TSR above 0.41 and has a maximum Cp that is less than half of Jooss et al. [2022b]. A possible reason why curves of higher buildings show bad performance with high TSR could be explained with the high level of turbulence that influence the aerodynamic of the turbine. It means that when the velocity of the turbine installed on high building increases it's easier that the performance of the the turbine drops.

The last figure regarding windward building is 4.18 and it shows only the high turbine on the model. Indeed, in this case the performances are drastically reduced in terms of TSR and Cp_{max}, the new values are respectively 0.3 and 0.1. There is no figure related to

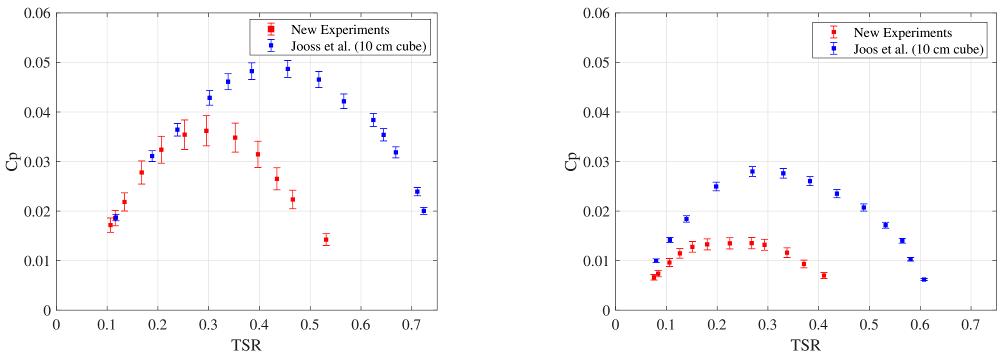

(a) High turbine (b) Low turbine

Figure 4.17: Position 2

low turbine on position 3 because the turbine doesn't spin, like it is stated in section 4.1. At that location indeed the turbine is completely inside the recirculation zone. Going on with the figures related of positions 4, 5 and 6 it's evident that the results of current experiments are more similar to the previous ones.

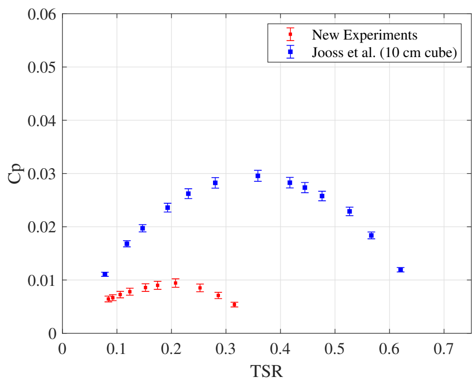

Figure 4.18: Position 3 high turbine

Looking at figure 4.19, it's evident that the Cp-TSR curves in both graphs are quite low due to the slow velocity of the flow in that particular position. As a result, both turbine configurations perform poorly. In particular, on the leeward building, the turbine fails to achieve high Cp and TSR, as the flow attempts to reattach on the leading edge. However, as we move towards the back of the square cylinder, at positions 5 and 6, the flow velocity tends to increase, as seen in figure 4.5. This is the reason why the curves tend to increase their Cp_{max} going toward the back positions. In figures 4.20a and 4.21a it can be noticed that in both the cases the current experiment on taller building perform slightly better than Jooss et al. [2022b]. On the other hands, the curves of the low turbine at positions 5 and 6 of the current experiments are superimposable on the curves of the previous experiment.

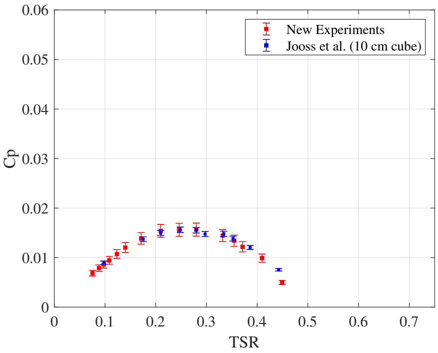

(a) High turbine

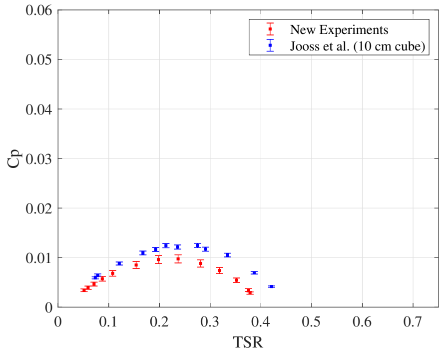

(b) Low turbine

Figure 4.19: Position 4

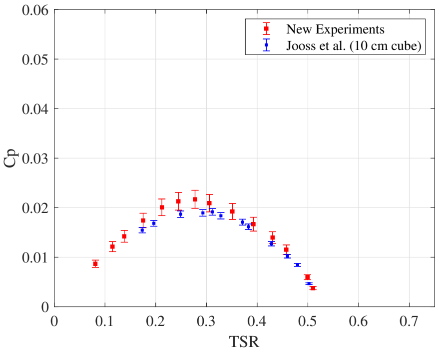

(a) High turbine

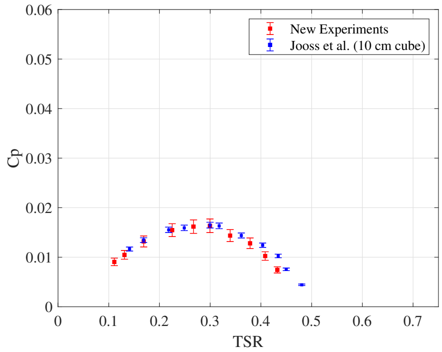

(b) Low turbine

Figure 4.20: Position 5

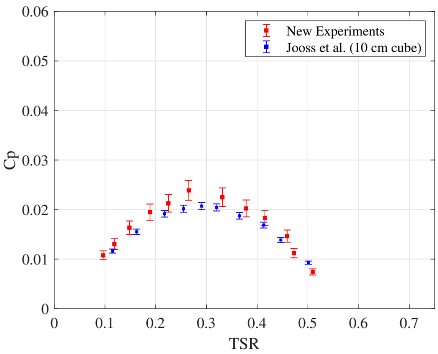

(a) High turbine

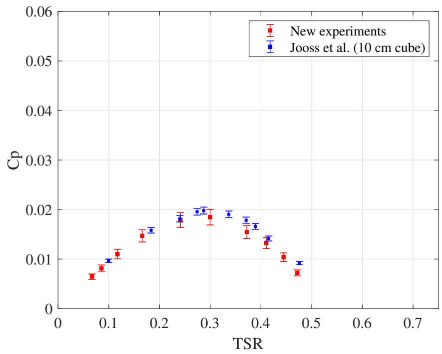

(b) Low turbine

Figure 4.21: Position 6

Chapter 5

Conclusions

At the end of this work, it is feasible to draw some conclusions regarding the flow field behavior around taller buildings and the performances of the turbine installed on them. In general, the flow field observed at the middle plane of the buildings is comparable to the one studied by Jooss et al. [2022b] but there are some variations that influence the Cp_{max} of the turbine. It is possible to summarize the analyses of the flow field on the windward building, see figure 4.4:

- The recirculation bubble on the square cylinder structure is thicker than on the cube, like is shown in 4.15, indeed that region is 12.3% higher than the previous one;
- The stagnation point in front of the windward building is very close to the artificial floor, around 7.5 cm above it and the vertical velocity w has lot of space to rise. The last one can be a reason why there is a difference between the heights of the recirculation bubbles;
- Over the recirculation zone there is still an acceleration zone but it is moved up due to the higher recirculation region;
- The turbulence profile get its max, in absolute value, on the central position (position 2);
- On ZY plane the velocity is not too much conditioned by 3D effects of the flow field and it remains almost constant going towards the lateral edge of the square building.

Another type of flow is visible on the leeward building, see figure 4.5:

- The flow tends to reattach on the leading edge and going towards the back of the model the velocity increases;
- The turbulence profiles at position 4, 5 and 6 start with high values close to the roof of the buildings and they maintain it for a quite large area on the Z axis;

- The highest value of the turbulence is at position 4;
- It is not visible a recirculation bubble on the roof of the model;
- On ZY plane it is visible that the velocity increases moving away from the middle plane.

After these general observations of the flow fields is possible to explain the behaviour of the turbine in different positions.

As evident from the table 4.2, in section 4.3, is possible to state that:

- the **turbine's performance on taller buildings** is **generally inferior** across various positions. This trend is **especially** pronounced **on the windward model** (positions 1, 2 and 3) where the recirculation zone is larger, and at position 3 where the low turbine is unable to rotate. However, there is one exception at position 1, where the high turbine configuration benefits slightly from an increase in flow velocity and therefore also its Cp_{max}.
- the **results** for **high turbine** configurations on the **leeward building** (positions 4, 5 and 6) **are positive**, with an increase of more than 10% observed for positions 5 and 6.
- **the worst results are observed for the low turbine configurations** on both the models where at each positions the performances are degraded. Indeed, the turbine is always completely inside the recirculation zone in the windward building and in the leeward building it is affected by the decelleration of the flow close to the roof.

The conclusion of this thesis highlights that there is no definitive or universal answer to the question of whether tall or small buildings are better for installing a small vertical axis wind turbine (VAWT). Many parameters, such as the heights of the structures on which the turbines are installed and the relative ratio to the rotor heights, must be carefully considered to ensure optimal turbine performance. The current study shows that performances are generally worst for turbines with small heights of shaft mounted on high-rise models buildings. Adjusting this parameter could potentially lead to better results. Anyway, in an urban environment, designing and selecting a location for a VAWT is a compromise that requires weighing different aspects.

Chapter 6

Further Work

At the end of this work lot of questions remain open and lot of work is necessary in order to understand the performance of VAWT in complex environments, like urban areas. There are more analyses that can be done in-depth about the subject matter of this thesis. A crucial aspect that needs improvement in this experiment is the construction of the models. Indeed the two model buildings are tall (along the z-axis) but their dimensions in x-direction and y-direction are still relatively small. Therefore, a larger building could better reflect a real application of VAWT mounted on the roof. Further improvements to the current experiments concern a deeper examination of the flow field. It would be important to investigate the flow in the cavity between the models and compare it to previous experiments conducted by Jooss et al. [2022a] and Martinuzzi and Havel [1999]. Additionally, a more detailed analysis of the flow field and velocity in the ZY plane could reveal any impacts resulting from the square buildings' edges. In the end, it could be studied the effect of changing the direction of the flow field (for different angles) and the turbulence intensity on the current experiment in order to make a comparison with previous experiments.

Bibliography

Wake structure of a finite circular cylinder of small aspect ratio. *Experiments in Fluids*, 37:720–730, 11 2004. ISSN 0723-4864. doi: 10.1007/s00348-004-0862-7.

World energy outlook 2022, 2022. URL https://www.iea.org/reports/world-energy-outlook-2022.

I. Abohela, N. Hamza, and S. Dudek. Effect of roof shape, wind direction, building height and urban configuration on the energy yield and positioning of roof mounted wind turbines. *Renewable energy*, 50:1106–1118, 2013. ISSN 0960-1481.

J. P. Abraham. *Small-Scale Wind Power : Design, Analysis, and Environmental Impacts*. Momentum Press, 2014. ISBN 1-60650-484-3.

J. V. Akwa, H. A. Vielmo, and A. P. Petry. A review on the performance of savonius wind turbines. *Renewable sustainable energy reviews*, 16(5):3054–3064, 2012. ISSN 1364-0321.

M. Bastankhah and F. Porté-Agel. Wind tunnel study of the wind turbine interaction with a boundary-layer flow: Upwind region, turbine performance, and wake region. *Physics of fluids (1994)*, 29(6):65105, 2017. ISSN 1070-6631.

A. S. Dar, G. A. Barcos, and F. Porté-Agel. An experimental investigation of a roof-mounted horizontal-axis wind turbine in an idealized urban environment. *Renewable Energy*, 193:1049–1061, 6 2022. ISSN 18790682. doi: 10.1016/j.renene.2022.05.035.

H. J. S. Fernando. Fluid dynamics of urban atmospheres in complex terrain. *Annual review of fluid mechanics*, 42(1):365–389, 2010. ISSN 0066-4189.

I. C. Gil-Garcìa, M. S. Garcìa-Cascales, and A. Molina-Garcìa. Urban wind: An alternative for sustainable cities. *Energies*, 15, 7 2022. ISSN 19961073. doi: 10.3390/en15134759.

IEA. Net zero by 2050 - a roadmap for the global energy sector, 2021. URL www.iea.org/t&c/.

IRENA. Rise of renewables in cities – energy solutions for the urban future, 2020. URL www.irena.org/publicationsrena.org/publications.

T. Ishugah, Y. Li, R. Wang, and J. Kiplagat. Advances in wind energy resource exploitation in urban environment: A review. *Renewable sustainable energy reviews*, 37: 613–626, 2014. ISSN 1364-0321.

A. R. Jha and A. Jha. *Wind Turbine Technology*. Power engineering / green technology. CRC Press, Hoboken, 2010. ISBN 1-4398-1506-2.

Y. Jooss. A fluid mechanic view on urban wind energy, 2022.

Y. Jooss, R. Bolis, T. Bracchi, and R. J. Hearst. Flow field and performance of a vertical-axis wind turbine on model buildings. *Flow*, 2, 2022a. ISSN 26334259. doi: 10.1017/flo.2022.3.

Y. Jooss, E. B. Rønning, R. J. Hearst, and T. Bracchi. Influence of position and wind direction on the performance of a roof mounted vertical axis wind turbine. *Journal of Wind Engineering and Industrial Aerodynamics*, 230, 11 2022b. ISSN 01676105. doi: 10.1016/j.jweia.2022.105177.

C. Kang, H. Liu, and X. Yang. Review of fluid dynamics aspects of savonius-rotor-based vertical-axis wind rotors. *Renewable sustainable energy reviews*, 33:499–508, 2014. ISSN 1364-0321.

A. KC, J. Whale, and T. Urmee. Urban wind conditions and small wind turbines in the built environment: A review. *Renewable energy*, 131:268–283, 2019. ISSN 0960-1481.

L. Ledo, P. B. Kosasih, and P. Cooper. Roof mounting site analysis for micro-wind turbines. *Renewable Energy*, 36:1379–1391, 5 2011. ISSN 09601481. doi: 10.1016/j.renene.2010.10.030.

J. F. Manwell. *Wind energy explained : theory, design and application / J.F. Manwell and J.G. McGowan, A.L. Rogers*. John Wiley, Chichester, 2nd ed edition, 2009. ISBN 9780470015001.

R. J. Martinuzzi and B. Havel. Turbulent Flow Around Two Interfering Surface-Mounted Cubic Obstacles in Tandem Arrangement . *Journal of Fluids Engineering*, 122(1):24–31, 11 1999. ISSN 0098-2202. doi: 10.1115/1.483222. URL https://doi.org/10.1115/1.483222.

R. J. Martinuzzi and B. Havel. Vortex shedding from two surface-mounted cubes in tandem. *International Journal of Heat and Fluid Flow*, 25:364–372, 6 2004. ISSN 0142727X. doi: 10.1016/j.ijheatfluidflow.2004.02.003.

J. F. McClean and D. Sumner. An experimental investigation of aspect ratio and incidence angle effects for the flow around surface-mounted finite-height square prisms. *Journal of Fluids Engineering, Transactions of the ASME*, 136, 2014. ISSN 1528901X. doi: 10.1115/1.4027138.

S. Mertens. Wind energy in the built environment : concentrator effects of buildings, 2006.

L. C. Pagnini, M. Burlando, and M. P. Repetto. Experimental power curve of small-size wind turbines in turbulent urban environment. *Applied Energy*, 154:112–121, 9 2015. ISSN 03062619. doi: 10.1016/j.apenergy.2015.04.117.

J. Pan, C. Ferreira, and A. van Zuijlen. Estimation of power performances and flow characteristics for a savonius rotor by vortex particle method. *Wind energy (Chichester, England)*, 26(1):76–97, 2022. ISSN 1095-4244.

I. Paraschivoiu. Wind turbine design : with emphasis on darrieus concept, 2002.

A. Sarkic Glumac, H. Hemida, and R. Hoffer. Wind energy potential above a high-rise building influenced by neighboring buildings: An experimental investigation. *Journal of wind engineering and industrial aerodynamics*, 175:32–42, 2018. ISSN 0167-6105.

A. P. Schaffarczyk. Introduction to wind turbine aerodynamics, 2020.

F. Toja-Silva, A. Colmenar-Santos, and M. Castro-Gil. Urban wind energy exploitation systems: Behaviour under multidirectional flow conditions - opportunities and challenges, 2013. ISSN 13640321.

L. Wang, D. Li, Z. Gao, T. Sun, X. Guo, and E. Bou-Zeid. Turbulent transport of momentum and scalars above an urban canopy. *Boundary-Layer Meteorology*, 150: 485–511, 03 2014. doi: 10.1007/s10546-014-9910-x.

A. J. Wheeler. *Introduction to engineering experimentation / Anthony J. Wheeler, Ahmad R. Ganji.* Prentice-Hall, Englewood Cliffs, 1996.

Wilson. Flow patterns over flat roofed buildings and application to exhaust stack design, 1979.

D. Wood. *Small wind turbines : analysis, design, and application / David Wood.* Green energy and technology. Springer, London, 2011. ISBN 978-1-84996-174-5.

D. Zajic. Flow and turbulence in urban roughness canopies, 2006.